EARTH SURFACE
Processes and Landforms

BSG British Society Geomorphology

Revisiting the morphological method in two-dimensions to quantify bed-material transport in braided rivers

SCHOLARONE™
Manuscripts

Revisiting the morphological method in two-dimensions to quantify bed-material transport in braided rivers

Gilles Antoniazza*, Maarten Bakker and Stuart N. Lane
University of Lausanne (Switzerland), Institute of Earth Surface Dynamics (IDYST)

0. Abstract

Research in the 1990s showed that bed-material transport rates could be estimated at the reach scale in both one-dimension and, over small spatial scales (10s of m), in two-dimensions. The limit on the latter was the spatial scale over which it was possible to obtain distributed data on morphological change. Here, we revisit the morphological method given progress in both topographical data acquisition and hydraulic modelling. The bed-material transport needed to conserve mass is calculated in both one and two dimensions for a 1600m x 300m Alpine braided river "laboratory". High-resolution topographical data were acquired by laser scanning to quantify Digital Elevation Models (DEMs), and morphological changes caused by the flushing of the water intake were derived from repeated surveys. Based on DEMs of differences, 1D bed-material transport rates were calculated using the morphological method. Then, a 2D hydraulic model was combined with a topographic correction to route sediment through the network of braided channels and to obtain a spatially variable estimate of transport in both downstream and cross-stream directions. Monte Carlo simulation was applied to the routing model parameters, allowing identification of the most probable parameter values needed to minimize negative transport. The results show that within-section spatial compensation of erosion and deposition using the 1D treatment leads to substantial local errors in transport rate estimates, to a degree related to braiding intensity. Even though the 2D application showed that a large proportion of the total transport was actually concentrated into one main channel during the studied low flow event, the proportion of transport in secondary anabranches is substantial when the river starts braiding. Investigations of the effects of DEM resolution, competent flow duration and survey frequency related to 'travelling bedload' and sequential erosion-deposition emphasized the critical importance of careful data collection in the application of the morphological method.

1. Introduction

The combination of high stream power, limited vegetation encroachment, wide accommodation space and a highly mobile bed allows braided rivers to rework their bed frequently, leading to high spatio-temporal variability in bed-material transport rates (e.g. Ashworth and Ferguson, 1986; Ashmore, 1991a; Ferguson, 1993; Tal and Paola, 2010; Zanoni *et al.*, 2008). Quantitative determination of morphological change and bed-material transport in such complex and dynamic environments has thus been a major challenge for fluvial geomorphologists (e.g. Ashmore and Church, 1998; Vericat *et al.*, 2017). Attempts have been made to predict patterns of erosion, deposition and transport in braided rivers based on physically-based, coupled hydraulics and sediment transport models, a 'forward method' (Church, 2006). However, multiple and complex interactions between unsteady water flow, a network of rough, non-uniform and unstable channels and changes in bed grain size distribution tend to make model predictions of erosion, deposition and transport highly uncertain (Haff, 1996). Whilst there is no doubt that general mechanisms of the braiding process may be captured in two-dimensional (e.g. Nicholas, 2003; Boroquez and Darby, 2008) or three-dimensional hydrodynamic models (e.g. Hardy *et al.*, 2005; Lane *et al.*, 1999; Nicholas and Sambrook-Smith, 1999), the system history implicit in braided rivers in the field makes their detailed quantitative prediction a challenge (Haff, 1996). A possible alternative is to infer bed-material transport rates using measurements of morphological change through time, labelled the 'morphological method' by Ashmore and Church (1998).

Recently reviewed by Vericat *et al.* (2017), the morphological method uses mass conservation to infer the changes in bed-material transport in space that are necessary to explain measured morphological change. A crucial limit to the success of this approach is the spatial and the temporal resolution of morphological data (Lane *et al.*, 1994; Fuller *et al.*, 2002; Lindsay and Ashmore, 2002). Work in the 1990s showed the morphological method to be feasible for inferring bed-material transport rates in braided streams (e.g. Ashmore and Church, 1998; Lane, 1997; Lane *et al.*, 1995). However, these studies were still limited by the time required to measure riverbed morphology (several hours up to a few days, even at low spatial resolution) using embryonic remote sensing approaches such as analytical photogrammetry (Lane *et al.*, 1994). In this context, Lane *et al.* (1994) showed significant bias in the estimation of volumes of morphological change if either the temporal or the spatial density of data collection does not match the rate of process change in time or space.

More recent developments in geomatics have speeded up data collection, initially using differential GPS (e.g. Brasington *et al.*, 2000) and digital photogrammetry (Chandler *et al.*, 2002; Westaway *et al.*, 2000, 2003) and more recently Structure from Motion (SfM) photogrammetry (e.g. Westoby *et al.*, 2012; Fonstad *et al.*, 2013; Javernick *et al.*, 2014; Bakker and Lane, 2017) and laser scanning (e.g. Fuller *et al.*, 2003; Heritage and Hetherington, 2007; Milan *et al.*, 2007; Williams *et al.*, 2014; Andersen and Pitlick, 2014). Such developments have allowed quantification of channel erosion and deposition patterns at higher spatial (centimetric) and temporal (hourly to daily) resolution (e.g. Lane *et al.*, 2003; Fuller *et al.*, 2003; Picco *et al.*, 2013; Williams *et al.*, 2014), providing data that can capture more closely the rate of change in process in space and time (e.g. Lane *et al.*, 1994; Vericat *et al.*, 2017).

The morphological method is based upon the Exner (1925) equation:

$$\left(\frac{\partial q_b^x}{\partial x}\right) + \left(\frac{\partial q_b^y}{\partial y}\right) + (1 - \varepsilon) * \frac{\partial_{z_{xy}}}{\partial_t} + \frac{\partial_{c_b}}{\partial_t} = 0$$

[1]

where q_b is the bed-material transport in the x and y downstream and cross-stream directions respectively, ε is the sediment porosity, z is elevation, t is time and c_b is the concentration per unit bed area of sediment in motion. Under the assumption that c_b is constant in space and time, [1] becomes in one dimension (Vericat et al., 2017):

$$\left(\frac{\partial_{Q_b}}{\partial_x}\right) + (1 - \varepsilon) * \frac{\partial_{\bar{z}}}{\partial_t} = 0$$

[2]

where Q_b is the section averaged bed-material transport rate and $\bar{z}$ is the section averaged net morphological change. Vericat et al. (2017) have reviewed thoroughly the application of [2] given the advent of high resolution topographic data. They show that the progressive improvement in the ease of data collection has removed many of the earlier practical obstacles that limited application of the morphological method. That said the fact that [2] implies integration across a section may lead to erosion and deposition within a section cancelling itself out, with the net within-section change hiding substantial within-section variability. We call this the spatial compensation effect, which may be particularly substantial in braided rivers where there is strong spatial variability in bed-material transport rate. Even if the spatial resolution of cross-sections downstream becomes very fine, there may be within-section spatial compensation. Thus, [2] is only an acceptable solution if a cross-sectionally uniform change in transport rate within a cross-section is assumed.

To deal with this problem, Lane et al. (1995) showed that it was possible to apply [1] in two dimensions (x and y), provided information is available to describe the (x,y) dependent divergence and convergence of sediment transport. They combined a two-dimensional (2D) hydraulic model to determine the divergence and convergence of flow with spatially distributed erosion and deposition data to estimate the spatial patterns of the time-averaged bed-material transport rate needed to conserve mass, for a very small (20 m x 8 m) area of a braided river. Although they proved the potential of the method, this scale was too small to explore the spatial structure of the bedload transport field. Associated with the progress made in high resolution topographic data acquisition, recent developments in Computational Fluid Dynamics (CFD) now enable successful hydrodynamic simulations of braided rivers in 2D to be performed over larger areas (kilometre-scale), at high resolution (tens of centimeters to a few meters) and with lower computational effort (about an order of magnitude quicker) (e.g. Bates et al., 2005; Williams et al., 2016). Thus, the 2D morphological method may now be a feasible approach over large areas and provide valuable information on the spatial structure of bedload transport in braided rivers without the challenges posed by fully coupled flow-sediment-channel change modelling (Haff, 1996).

The aim of this paper is to revisit the morphological method in 2D, profiting from developments in remote sensing and computational techniques over the last 20 years. We apply the morphological method in both 1D and 2D to a 1600 m by 300 m stretch

of an Alpine braided river, and demonstrate what additional information the 2D approach provides as compared with the 1D treatment. We test and discuss the elements of data collection and model parameterization that affect the calculation of transport rates based on the 2D morphological method and that should be considered carefully in any geomorphological application. These include the sensitivity of the parameters used in the 2D sediment routing, such as DEM spatial resolution, competent flow duration, 'travelling bed load' (Piton and Recking, 2017) and sequential erosion and deposition through time between surveys (Lindsay and Ashmore, 2002). We then use the results to explore the spatial structure of bedload transport in the investigated setting to illustrate the potential of the method.

2. Methodology

2.1 Methodological approach and field site

Whilst the acquisition of high resolution topographic data has progressed significantly in recent decades (e.g. Brasington *et al.* 2003, 2012; Lane *et al.*, 2003; Westoby *et al.*, 2012; Fonstad *et al.*, 2013; Williams *et al.*, 2014; Vericat *et al.*, 2017), these approaches continue to face four challenges for application to rivers (Lane, 2000): (1) there remain problems with the representation of inundated zones, which many techniques still fail to capture adequately; (2) significant time may be required to survey such zones or to obtain the calibration data necessary to apply remotely sensed methods (e.g. Westaway *et al.*, 2003); (3) net morphological change is dependent upon the flow processes between measurements and the potential sequential erosion and deposition that may occur between the dates of measurement (Lane *et al.*, 1994; Lindsay and Ashmore, 2002); (4) there is the challenge of 'travelling bedload', where bedload travels through a reach of river without having any morphological expression and so which is not captured through repeated topographic surveys (Piton and Recking, 2017). In terms of (2) and (3), as ∂t tends towards zero, the standard deviation (in time) of bed-material transport should rise until the point at which all timescales of variability have been captured. This may well be at the timescale of movement of individual grains, which is clearly not feasible. Two points follow. First, these problems are a reminder that the morphological method does not provide a conventional estimate of bedload transport. Rather, it gives the change in bedload transport rate over a given time period (i.e. between surveys) necessary to conserve mass. Second, for such estimates of change in bedload transport rate to be of value, the measurement of morphological change needs to be reliable, including both its spatial and temporal resolution.

In this paper, we profit from a braided river 'laboratory', the Borgne d'Arolla (Valais, Switzerland), which resolves the problems of inundated zones. The study reach is 1600 m long, extending downstream from the Lower Bertol flow intake (Figure 1). The bed slope is on average 6% and the bed-material is relatively coarse with a D_{50} between 18 and 35 mm (Warburton, 1992; Bakker *et al.*, 2018). The Borgne is subject to almost total flow abstraction associated with hydroelectric power production (HEP). This results in prolonged periods when the river bed is dry, bounded by short duration flushing flows that mimic low magnitude flood events and which rework the braided channel network. Morphological changes can be accurately measured by surveying the area when the bed is dry between two flushing events. The flushing frequency is largely a function of glacier melt rates, and because sediment production rates are high

in this basin (Warburton, 1992; Bakker *et al.*, 2018), flushing frequency is daily to weekly in the early summer and autumn, rising to twice or more per day during the mid and late summer. Clearly, this is an artificial system, notably because of the sharp change between dry conditions and the arrival of a wave of water and sediment once the intake opens. This may affect flow and sediment dynamics, especially in the upstream part of the reach closer to the water intake. This disadvantage is countered by the fact that it is possible to measure the bed when it is dry, avoiding the problems of inundated areas, similar to flume simulations of braided rivers that are drained periodically to allow bed measurement (i.e. Ashmore, 1982, 1988; Hoey and Sutherland, 1991). By using the flushing discharge data provided by the owner of the hydropower scheme, we also have a mean for estimating both the discharge and the minimum sand and gravel volumes delivered during each event (Bezinge *et al.*, 1989; Lane *et al.*, 2017; Bakker *et al.*, 2018).

In this section, we detail: (1) the topographic data acquisition and processing needed to determine z_{xy} in [1] and [2]; (2) the upstream boundary data that were obtained for water and sediment delivery); (3) how the hydraulic model was set up, calibrated and validated; (4) its use to estimate water depths and flow velocity fields; and (5) the calculation of 1D and 2D bed-material transport rates, the application of both [1] and [2] to our data. To keep the methodology brief, we use supplementary on-line material to provide full methodological detail.

2.2 High resolution topographic surveys and data processing

Topographic data were acquired using an ultra-long range, near-infrared terrestrial laser scanner, the Riegl VZ 6000. The entire study area could be scanned from a single vantage point 1.2 km from the downstream end of the study area (Figure 1) aided by, the elevation of the scanning point 200 m above the study reach and the relatively straight reach with little vegetation and where banks and bars did not hide significant areas of the bed from the scanning point. Given the high frequency of flushing and the lack of an easy access vantage point elsewhere, cross-scanning from an opposite direction was not feasible. Therefore, because of the long base-line and of the single scanning vantage point, a careful adjustment of the point clouds as well as a robust uncertainty analysis were required to avoid bias and noise in the data.

Field data collection was undertaken in August 2013, when high rates of ice and snow melt resulted in frequent flushing events. A total of 4 scans of the studied area were undertaken (Table 1). The instrument was operated at a low frequency (50 kHz) to maximise returns from more distant parts of the study area, using a measurement step of 0.005° and resulted in an average point spacing of c. 0.1 m at 1.2 km and 0.3 m at 3 km, the downstream and upstream boundaries of the study area. The instrument acquires data very rapidly (>20'000 per second) and the quality of relative positioning at the distances of interest here is excellent (accuracy of 15mm, precision of 10mm). From the scan site on the hillside, it took an average of 8 minutes to scan a surface of c. 500'000 m².

The general approach to post-processing and adjustment of scans follows Gabbud *et al.* (2015). The surface area of the scan reflected not only the spatial extent of the study area but also the need to have stable zones outside the active channel that were used to co-register acquired point clouds. The scan area was set to include infrastructure

(e.g. buildings, bridges) on all sides of the study area to allow the registration of each scan, using the first scan obtained on the 1st August 2013 as reference (Table 1). Each scan produced a point cloud. After manual editing to remove outliers related to, for example, atmospheric reflections due to dust or moisture, we undertook an initial co-registration of the data onto the 1st August survey. Small numbers (c.10) of common, stable, patches of data points (e.g. buildings, bridges) were identified manually. Then, an IDW iterative algorithm (Zhang, 1994) was used to obtain an exact co-registration, minimizing the standard deviation between all points in the stable patches was within the range ±0.05 m following Gabbud *et al.* (2015). The associated residuals were checked to make sure that they were Gaussian with a mean of zero in order to avoid bias and to allow eventual propagation of error (Lane *et al.*, 2003). Table 1 gives the details of each scan and results of the registration. DEMs were created by interpolating onto a collocated grid using kriging (Fuller *et al.*, 2003). With well-adjusted collocated grids, the DEMs could be directly compared as DoDs.

However, as co-registration only removes systematic error, and given that river-bed surfaces are heterogeneous, there will remain a sample density related error (e.g. Lane, 1998a; Fuller *et al.*, 2003; Heritage and Hetherington, 2007). Thus, an additional uncertainty assessment was required. To each individual Digital Elevation Model (DEM) we applied a cell-by-cell error estimate based on both the point cloud density and the aspect of each cell with respect to the scan direction[1] included in a Fuzzy Inference System (Wheaton *et al.*, 2010). Then, we propagated the individual cell DEM error into the corresponding cell of the DEM of Difference (DoD) and applied probabilistic thresholding of measured topographic change data based on the uncertainty estimate. This method follows Lane *et al.*, (2003) and Wheaton *et al.* (2010) and is fully described in the Supporting Online Material (S1).

2.3 Hydrological and sediment delivery data

The method used to reconstruct water and sediment releases for each flushing event follows Bezinge *et al.* (1989), Lane *et al.* (2017) and Bakker *et al.* (2018). Through collaboration with the hydroelectric scheme operators, we had access to high quality, 15 minutes frequency, discharge data[2] released from the Lower Bertol intake at the upstream boundary of the study reach (Figure 2), which allowed us to derive flushing discharge and duration. The intake has two separate sediment traps for coarse sediment (gravel and coarser) and fine sediment (finer than gravel). The duration of flushing the gravel trap was more than 60 minutes while that of the sand trap was typically between 15 and 45 minutes. Thus, it was possible to distinguish flushing events from these traps in the flow hydrograph (Figure 2). A flush is triggered automatically once a given threshold of sediment is reached in the trap. Knowing the volume of the traps at that threshold (150 m^3 for the gravel trap and 7 m^3 for the sand trap; Bezinge *et al.*, 1989), the sediment packing density in the traps (1300 kg/m^3 based on measurement of Bezinge *et al.*, 1989), and assuming the flushing event will

---

[1] Note that the use of 'point density' and 'aspect' as proxies for the uncertainty is relevant for this specific field setup with a single TLS scanning vantage point, but may not be sensible for studies using different techniques and/or field settings.

[2] Data cannot be made public for commercial reasons. However, they can be made available upon request.

last as long as the time required to empty it entirely, the mass of sediment released to the system for each event could be estimated. Table 2 summarizes the amount of sediment released into the system within each scan interval (cumulated volumes of a sequence of flushes) and individual flushing records are available in the Supplementary Information (S2). Bezinge *et al.* (1989) reported a variation in sediment volumes released by each event of about 15% for both the sand and the gravel trap. This variation was used to define an uncertainty range of the released volume estimates for each event (Table 2, Supporting information S2). Since 2008, the coarse sediment trap has also been flushed preventatively during the night (at 23:30) if the accumulated sediment reaches 60% of the trap capacity. Thus, night-time events have additional uncertainty that was propagated into the uncertainty range in Table 2 and Supporting Information (S2). The type of flushing event is important for the application of the morphological method, as gravel purge (larger volume, longer duration) tend to produce more morphological expression while sand purges tend to be washed through.

Ideally, the study reach would be surveyed after each event in order to derive morphological change associated with individual events and minimize the effects of sequential erosion-deposition through time (Lindsay and Ashmore, 2002). However, both the timing of events (often in the middle of the night) and the unpredictability of the triggering (most of the events start automatically once a given threshold is reached) made this impossible and for this reason most of the intervals between surveys include more than one event (Figure 2). Note also that during flushing, especially the night-time events, the intake may be left open for a period longer than that required to empty it, so that there is a larger throughput of sediment that cannot be considered. In general, therefore, the input of sediment we estimated into the study reach (Table 2, Supporting Information S2) should be considered as a minimum value.

2.4 Hydraulic modelling

Lane *et al.* (1995) showed it was possible to apply the morphological method in two dimensions provided sediment can be routed through the braided channel network. To do so, we used a 2D hydraulic model to obtain water depths and flow vectors and derive inundated channels and shear stress fields. Model setup, calibration and validation steps are presented in the following sections.

2.4.1 Model description

Hydraulic simulations were performed in the open source Basement code (version 2.7, http://www.basement.ethz.ch/), which was designed to perform stable numerical simulations in Alpine rivers, and whose use is therefore suitable in the field setting of this project (Faeh *et al.*, 2011). Structured simulation grids were created with the 3D surface modelling software SMS (version 12.2) at a resolution of 2 m, considered as a good compromise between model stability, process representation and computational efficiency. The 2D Basement model was parameterized with the standard physical values found in the literature (e.g. Faeh *et al.*, 2011), that is a gravitational acceleration of 9.81 m^2/s, a molecular viscosity of $1e^{-0.06}$ m^2/s and a fluid density of 1000 kg/m^3. Here, we applied a constant discharge, which was set as the maximum value recorded during the period considered (Table 2), and ran the model long enough to reach steady conditions in the system. Note that data suggest that this maximum is reached rapidly when flushing begins, and flushing stops abruptly once the intake is empty. To avoid semi-wetted cells and numerical instabilities, a minimum water depth of 0.05 m was

required for a cell to be defined as inundated (Ingham and Ma. 2005). Simulations were performed with a fixed bed of the initial topography (first DEM of the survey period) for numerical stability reasons and because the main interest of running a 2D model was to get for each survey period two-dimensional spatially variable water depths (Figure 3a) and flow velocity vectors (Figure 3b) along the study reach. This is an important limit of this study as bed-material transport and bed reworking will modify hydraulic conditions continually (e.g. Nicholas *et al.*, 1995, Mosselman, 2005). More details about the model parameterization are available in the Supporting Information (S3).

2.4.2 Flushing event calibration and validation

There are serious uncertainties regarding the extent to which grain size can be readily transformed into a roughness parameter in braided rivers due to the presence of macro-roughness such as bedload sheets, dunes or bars that are not taken into account when deriving the roughness from a surface grain size (Nitsche *et al.*, 2011). Their effect on the water depths and flow velocities is difficult to quantify. As a consequence, a spatially homogeneous bed roughness was used in the model as the only calibration parameter for flushing propagation velocity. The space-time propagation of water flow was determined for 5 flushing events in early August 2013, during which we took pictures of the wave front at regular intervals, assuming that the discharge rose rapidly to its peak values in each release.

The first three flushing events were used to calibrate the model, and the last two for the validation process (Lane *et al.*, 2005). With a Manning's *n* of 0.06, minimum delays in average wavefront propagation ($4s$) were found, and modelled velocities tend to be overestimated in the upstream part of the reach (0 m to 600 m) and underestimated in the downstream part (950 m to 1600 m). This is likely to be a consequence of using a spatially uniform roughness, and reflects measurements of downstream fining within the reach (Warburton *et al.*, 1992; Bakker *et al.*, 2018). That said, the errors are small, and validation with *n* = 0.06 for two other flushing events showed on average an even smaller difference between the real and the modelled events ($2s$). Therefore, every simulation in this paper was run with a spatially uniform Manning's *n* of 0.06. Detailed description of the calibration and validation steps is available in the Supporting Information (S2).

2.5 Morphological method

2.5.1 1D application

When one of the boundary fluxes is known (i.e. system input or output), net volume changes per cross-section measured by DEM differencing (Lane, 1998a) are calculated as the balance between erosion and deposition within that cross-section (Vericat *et al.*, 2017). Then, cross-section volume changes are routed from cross-section to cross-section, starting from the known sediment boundary flux following Ashmore and Church (1998). To do this, [2] was discretized as:

$$S_j = S_{j-1} - \frac{\sum \rho\,(1-\varepsilon)\Delta x_j \Delta y_j\,\Delta z_j}{t_c}$$

[3]

where S_j is the transport rate per second [kg/s] for a given cross-section j, S_{j-1} is the transport rate coming from the upstream cross-section (in case of a routing from upstream), ρ is the material density [kg/m³], $(1-\varepsilon)$ the porosity [-], $\Delta x_j \Delta y_j\,\Delta z_j$ the net volume change by cross-section measured by DEM differencing and t_c the duration of competent flow [s] based on flow records (Table 2, Supporting Information S2). As flushes rise rapidly to the peak discharge and stop abruptly when the intake is empty, we assume the flushing duration to be a good estimate of competent flow duration. However, competent flow duration may be underestimated if the flow is not competent for the entire flushing duration, due to a slower rising limb for instance. On the other hand, flushing may also be competent for a longer period than the flushing flow duration if there is flow attenuation and the hydrograph tail still enables transport once the intake is closed. Uncertainty in the estimate of competent flow duration is important because it will scale the transport rates estimates as morphological changes are integrated through time in [3] (Lane *et al.,* 1995; Vericat *et al.*, 2017).

We used a material density of ρ = 2650 kg/m³ and a porosity of $(1-\varepsilon)$ = 0.18 following Carling and Reader (1982). The initial transport rate for each flushing event at the upstream boundary of the system was based on the estimations of the associated minimum mass released from the sediment traps (Table 2). The result is a cross-section average rate of transport [kg/s]. If the upstream sediment supply condition is high enough, then the predicted sediment transport rate should be positive throughout the reach (i.e. the no-negative sediment transport condition, where more material is supplied in transport from upstream than gets deposited, Lane *et al.*, 1995). It is possible that there is sediment transport through the reach that is not expressed morphologically (Piton and Recking, 2017). However, if the upstream sediment supply is correct, the maximum possible rate of 'travelling bedload' is the minimum transport rate estimated using the 1D morphological method. If the minimum is negative or zero, there is sufficient deposition to balance all supplied sediment and there can be no bedload that has no morphological expression. It is also important to note that in our case, for sediment going through the system without involving neither erosion nor deposition during events of 15-120 minutes, it would mean that particles would need to travel on average faster than 1.8 m/s and 0.2 m/s respectively to pass through the

1600 m reach without involving neither erosion nor deposition. This is unlikely, where the average flow velocity in the simulations is 0.4 m/s.

2.5.2 2D application

Application of the morphological method in two-dimensions requires data derived from the hydraulic model to route the sediment cell-by-cell through the network of braided channels (Lane *et al.*, 1995). Application of [1] is based upon routing the morphological change in the *x* and *y* directions adding or subtracting according to each Δz_{xy} and using the same porosity treatment as in [3]. The basic principle behind the sediment routing is that the trajectory of sediment is a function of the resolution of two vectors representing flow direction and topographic forcing, each expressed as a shear stress:

$$\tau_R = \tau_B + \tau_G$$

[4]

where *R* is the resultant shear stress (τ, Nm^{-2}) acting on the stream bed and *B* and *G* indicate the flow-related and the topographical- or gravity-related components respectively.

The flow-related shear stresses τ_B were simulated in Basement based on the depth-averaged flow velocities and using a quadratic friction law in both *x* and *y* directions (Ingham and Ma, 2005; Lane, 1998b, Ferguson, 2010), such that:

$$\tau_B^x = \rho \frac{gn^2}{h^{1/3}}|v|v_x$$
$$\tau_B^y = \rho \frac{gn^2}{h^{1/3}}|v|v_y$$

[5]

where $|v| = \sqrt{v_x^2 + v_y^2}$ is the magnitude of the velocity vector, ρ the water density [kg/m^3] and with *g* is the gravitational acceleration [m/s^2], *h* the water depth and *n* the calibrated Manning's n (Ingham and Ma, 2005).

To represent the effects of deviation between the flow and sediment transport directions due to topography forcing τ_G (e.g. Mosselman, 2005), we apply the classic formulation of van Bendegom (1947), widely used for sediment routing in gravel-bed rivers (e.g. Ikeda, 1989; Nelson and Smith, 1989; Struiksma and Crosato, 1989; Mosselman, 2005; Engelund 1974). The topographic component of shear stress τ_G is given by the increase in the bed shear stress above the critical shear stress due to the fact that sediment is not on a flat slope and so is topographically-forced (after Nelson and Smith, 1989):

$$\tau_G^x = \tau_c \frac{\sin\alpha \; s_x}{\sin\phi_o |s|}$$
$$\tau_G^y = \tau_c \frac{\sin\alpha \; s_y}{\sin\phi_o |s|}$$

[6]

where τ_c is the critical shear stress defined from a Shields condition, α is the arctan of *s*, the bed-slope derived from the DEM at the start of the period which can also be resolved into *x* and *y* directions; and ϕ_o is the bulk angle of repose of the sediment. Application of [4] through [7] gives the 2D form of the morphological method:

$$q_b^x = \frac{1}{t_c} \frac{\tau_R^{x^2}}{\tau_R^{x^2} + \tau_R^{y^2}} \left[\sum_{k=1}^{8} q_b^k + \rho(1-\varepsilon)\Delta x \Delta y \Delta z_{ij} \right]$$

$$q_b^y = \frac{1}{t_c} \frac{\tau_R^{y^2}}{\tau_R^{x^2} + \tau_R^{y^2}} \left[\sum_{k=1}^{8} q_b^k + \rho(1-\varepsilon)\Delta x \Delta y \Delta z_{ij} \right]$$

[7]

where t_c is the duration of competent flow and *k* are the 8 cardinal cells that could deliver sediment to cell *ij*. All cells require at least one cardinal cell that they deliver sediment to. Note that when applying [7], if a cell is calculated as having negative transport, that is more sediment being deposited than supplied, the transport rate is set to zero to avoid negative transport being propagated downstream.

The main problem with this analysis is the introduction of parameters in [7]. With a spatially-distributed homogenous sediment on the stream bed, the critical shear stress and the angle of repose should be spatially and temporally homogeneous (similar to Manning's *n* in [5]). Whilst the DoDs can provide Δz_{ij}, they yield no information on the sediment composition. Here, we make an explicit assumption of homogeneity and then determine the spatially uniform values of these parameters (i.e. critical shear stress, angle of repose, Manning's *n*) that minimises the number of cells with negative transport. The zero negative transport rule is more stringent in this application as there are many more cells that may become negative than in a 1D application (the number of cross-sections used). The probability of encountering negative transport may result from either insufficient sediment supply from upstream (e.g. the throughput of sediment when the intake is flushed for a longer period than the time required to empty the intake, or the shorter duration of competent flows compared to total flushing duration) or from errors in the sediment routing, whether due to the form of [7] or uncertainties regarding the parameters in [5] or [6]. In this application we use a Monte Carlo Generalised Likelihood Uncertainty Estimation (GLUE) approach (after Beven and Binley, 1992) to quantify the relationship between randomly sampled parameter values and the no-negative transport condition. We quantified the percentage of cells experiencing negative transport for different realisations by sampling upstream boundary sediment supply [m³], angle of repose [°], critical shear stress [Nm⁻²] and Manning's n [-]. Each parameter was sampled randomly in a range of plausible values to produce 2000 model realisations in total. This allowed us to determine the most probable combination of parameters required to minimize the proportion cells with negative transport.

2.5.3 Comparison of 1D and 2D approaches

To summarise, the 1D and 2D applications of the morphological method are compared in Figure 4. The location and volumes of erosion and deposition over the floodplain are presented in Figure 4a. The scheme in Figure 4b illustrates how with the 1D method,

it is possible to have net erosion, net deposition or net balance within a section even though some cells in the section may be eroding and some depositing. The scheme in Figure 4c shows how by using the wetted area to constrain volume estimates, possible errors (change in non-inundated areas) can be accounted for (striped cell in Figure 4c). Note that integration of the 2D calculation across a section by definition gives the 1D result, except locally when there is lateral transport within a section. In this case, only the cells providing sediment downstream should be used for integrating sediment transport along the cross-section. The non-negative transport condition is also presented in Figures 4b and 4c when sediment input is reduced. In the 1D case, it gives the minimum amount of sediment required to have no-negative cross-sectional transport over the reach (+2 m^3 in the example). In the 2D case, it shows the location and number of cells experiencing negative transport given the sediment input.

The application of the morphological method in two-dimensions enables a spatially-variable estimate of bed-material transport rates in both downstream and cross-stream directions (Lane *et al.*, 1995, Figure 4c). By calculating morphological change as a balance between erosion and deposition within each cross-section, the 1D approach (Figure 4b) is likely to miss important information about local conditions of transport if both erosion and deposition are occurring simultaneously within a cross-section, which is likely in alluvial channels, and in particular in braided rivers (e.g. Lane *et al.*, 1994, 1995): the problem of spatial compensation. In this paper, we quantify the volume of spatial compensation of erosion and deposition that is locally unaccounted in the 1D calculation as compared with the 2D approach. Over a given cross-section, local errors in the 1D approach will be greater if the net changes (volume of erosion + volume of deposition) tend towards 0 while the gross changes (|volume of erosion| + volume of deposition) become greater. The difference between gross change and |net changes| divided by gross change therefore gives the proportion per cross-section of the volume change that will locally not be accounted into the 1D calculation as compared with the 2D approach.

2.5.4 Implications of the 2D morphological method for braided rivers

To understand where the spatial compensation of erosion and deposition occurs, and to investigate the link between the 2D spatially-variable estimate of transport and the braiding process, two additional metrics where derived from the data. First, the number of anabranches per cross-section was calculated based on the model inundated area (occurrence of dry-wet cell transition) and is considered as an expression of braiding intensity. Second, an anabranch ranking was performed by summing over the cross-section the transport contained in each separate anabranch (cells contained within dry-wet transitions), and numbering the anabranches from highest to lowest transport rate.

2.5.5 Impacts of topographic survey resolution in time and space

We investigate the effect of DEM spatial resolution and surface complexity on the transport rate estimates by interpolating the initial Lidar point cloud at 0.5 m, 1 m and 2 m, and systematically calculating the associated transport rates in [3] and [7]. Simulated water depths and flow fields were downscaled to 1 m and 0.5 m from the 2 m calibrated simulations to be able to isolate the effect of spatial resolution on the application of the morphological method.

We investigate the effect of scanning frequency (i.e. the problem of sequential erosion and deposition between survey dates) on the transport rates estimate by calculating morphological changes and associated transport rates for the same period 1st-6th August (Table 2), but with various scanning intervals, and therefore different degrees of sequential erosion-deposition. For the two survey case (period 5 in Table 2), morphological changes were derived from one DoD, and transport rates were calculated according to [3] adding the sediment input associated to the 22 flushes and integrated through the competent flow duration of these 22 events. For the more-than-two survey cases (Table 2, addition of periods 1, 2, 3 and 3, 4 respectively), morphological changes associated to multiple pairs of scans were summed-up, before adding the sediment input and integrating them over the duration of competent flow of the same 22 flushing events (Table 2) to calculate transport rates. This results in directly comparable morphological changes and transport rates for a single period that illustrates the effect of survey frequency upon the application of the morphological method.

3. Results

3.1 DEM differencing

Morphological changes derived from DEM differencing (Table 1) between the first (1st August) and the last Lidar survey (6th August) are shown in Figure 5 to illustrate the derivation of a DoD and the detectable morphological changes induced by a series of 22 flushes of the water intake (period 5 in Table 2). There are patches of both erosion (red) and deposition (blue), that often have an elongated shape in flow direction, and which show up to 1 m elevation change in both directions. The occurrence of both erosion and deposition within the same cross-section is not uncommon, which will affect the suitability of the 1D application of the morphological method (Lane *et al.*, 1995). We chose the 3rd to 4th August to further apply the morphological method because it had the smallest number of flushing events (1 gravel, 2 sand) and is therefore expected to be affected the least by sequential erosion and deposition between scan dates (Lindsay and Ashmore, 2002).

3.2 1D Bed-material transport rate

1D transport rates were calculated using [3] for the period 3rd to 4th August. The upstream input of sediment into the system was determined based on flushing data (Table 2). When the slope of the transport rate versus distance is positive in Figure 6 (e.g. between 600 and 850 m), the river is eroding and so contributing bed-material to transport. When it is negative, the river is depositing sediment (e.g. between 850 and 1000 m). The 1D approach allows estimation of the spatial variability in the transport rate in the downstream direction, and determination of the output of sediment from the system (about 15 kg/s in this case). The minimum value of bedload transport is estimated at around 1400 m downstream at 0.5 kg/s and this is the maximum rate of 'travelling bedload', that is bedload transport that has no morphological expression.

3.3. Parameter sensitivity analysis of the 2D bed-material transport rate

The 2000 iterations of the Monte Carlo sensitivity analysis were performed for the 3rd to the 4th August period, according to the parameter ranges defined in Table 3, which are enveloping sensible values for those variables. We ranked each parameter set by its associated negative transport condition, defining the lowest as best. The mean and standard deviation of parameter values associated with each ($n + k$) ranks of the negative transport condition is plotted in Figure 7 against the mean value of the condition for those ranks, for $n = 20$ and $k = 0 : 2000-n$. The mean and standard deviation of parameter values resulting from the Monte Carlo sensitivity analysis are shown in Figure 7. On each plot, the position with the largest standard deviation (the right hand side) corresponds to the mean and standard deviation of the full set of each parameter value used in the simulations. As the negative transport condition declines (i.e. right to left on the x-axis), if the standard deviation narrows, it suggests that selecting a narrow range of the parameter leads to better simulations. For instance, selecting those runs that have higher sediment supply leads to an improvement the mean negative transport condition associated with those runs. For the topographic forcing parameters, selecting runs with the critical shear stress closer to c. 40 Nm^{-2} (bottom left) and those with Manning's n closer to c. 0.07 (bottom right) improve the model simulations, whereas the negative transport condition is less sensitive to change in the angle of repose for a mean angle of c. 31° (top right). Based on results in Figure 7, we optimized the model with the no negative transport condition by setting an angle of repose of 31°, a critical shear stress of 40 N/m^{-2}, which corresponds to a D_{50} of about 32-64 mm (Julien, 2002). Then, we used the mean sediment supply volume (160 m^3) as upstream supply, which is very close from the estimate from the water intake (164 m^3, period 2 in Table 2). Finally, we used a Manning's n of 0.07, which is close from the calibrated value we found in the hydraulic model (0.06).

With this parameterization, 9% of the cells remain with negative transport. This rises to 10% if upstream supply is removed. If we introduce upstream supply at this rate but remove topographic forcing by setting the critical shear stress to zero, the figure rises to 11% (Figure 8a). If upstream sediment supply is also removed, it increases it slightly more (Figure 8b). Comparison of these two scenarios shows how topographic forcing is responsible for increasing the lateral component of sediment transport in a way that slightly reduces the extent of negative transport, but also locally increases the level of braiding. The model appears to be more sensitive to the roughness than to the critical shear stress, as the amount of negative cell rises up to 18% if Manning's n and upstream supply are set to zero while critical shear stress is maintained to 40 Nm^{-2}. If the number of cells affected by negative transport is quite considerable, note that in term of volume of transport it is very low (from 10^{-6} to 10^{-5} %).

3.4 Estimations of 2D transport rates

Visualization and analysis of sediment transport in two dimensions (Figure 9) shows substantial within cross-section variation in transport rates, as well as zones of convergence and divergence of transport. Higher rates of transport (values between 2.5 and 5 kgm^{-1}s^{-1}) are found in single-thread channels (i.e. 170 m – 200 m, 900 m – 950 m, labelled A) but also in multiple braided channels (i.e. 300 m – 800 m, 1000 m – 1200 m, labelled B), showing the ability of the river to rework the bed locally, even when the river flow is not concentrated in a single channel. Lower rates of transport (values between 0 and 2.5 kgm^{-1}s^{-1}) are commonly located where the river braids, but also in single-thread channels towards the downstream half of the reach (1400 m –

1450 m, labelled C) where rates of transport are generally decreasing. Even though many secondary anabranches are active all along the reach during this flushing event, transport appears to be mainly focused into one main anabranch (except between 650 and 750 meters where transport spreads evenly into two anabranches, labelled D).

3.5 Comparison of 1D and 2D approaches

When considering the reaches with a higher braiding intensity (greater number of anabranches, especially between 400 m - 800 m, 900 m – 1200 m, 1400 m – 1550 m), some variability in transport rates between channels for the same cross-section remains (Figure 9). Such variability is not captured through the 1D treatment. The 1D calculated transport rate differs most from the 2D calculations when there is both erosion and deposition within a section. This is represented in Figure 10 by comparing the gross change to the net change, as well as the number of anabranches, against distance downstream. The excess in percent of the gross over the net change ranges from 0% to 90% of the volume change per cross-section, 48% on average over the reach, and we label this the local unaccounted volume change in the 1D approach.

The unaccounted volume change per cross-section tends to be positively correlated with the number of anabranches (r = 0.43, p < 0.05), indicating that the higher the braiding intensity, the greater the probability of within-section spatial compensation of erosion and deposition (e.g. 400 m – 800 m; 1400 m -1550 m). However, this correlation is not perfect: locally, there are large volumes of unaccounted change in the 1D approach where the number of anabranches is lower. That is, there is spatial compensation of erosion and deposition within inundated cells of a single-thread channel (e.g. 1300 m). Similarly, relatively low degrees of spatial compensation effects in sections are present when anabranch number is relatively large (e.g. 600 m), when all the anabranches of a cross-section either consistently erode or deposit.

3.6 Implications of the 2D morphological method for understanding braided rivers

The 1D total transport for period 3rd to 4th August (black line), the 1D transport in the main channel (blue line) and 1D transport in the secondary anabranches (red shading) are determined in Figure 11a on the basis of the 2D calculations. The blue shading is the symmetrical inverse of the red shading. Where there is no blue or red shading, all of the transport takes place in a single thread, and globally the narrow blue shading confirms that most of the transport tends to take place in one main anabranch. For this survey interval, the proportion of transport taking place in the main anabranch is 87 %, and it goes up to 98 % if we consider the main two anabranches. In some areas, however, transport is distributed between two (e.g. at c. 400 m) or more anabranches (e.g. 550 – 600m). Where the river braids, the proportion of the transport taking place in secondary anabranches is locally substantial (Figure 11b). It ranges from 0 to 64 %, 15 % in average over the reach. The proportion of transport taking place in secondary anabranches is positively correlated with the anabranch number (r = 0.52, p < 0.05), which suggests that the river is locally able to successfully redistribute and transport the sediment within multiple anabranches, to a degree proportional to braiding intensity.

3.7 Methodological considerations

3.7.1 The effect of DEM spatial resolution

With increasing DEM spatial resolution, the level of surface complexity that is captured in the DEM increases, while low resolution DEMs tend to smooth the topography. Therefore, the morphological change measured through DEM differencing is typically larger with greater DEM resolution; we found increases of respectively 23% and 5% when we increased the DEM resolution from 2 m to 1 m and from 1 m to 0.5 m. 1D transport rates calculated through the application of the morphological method using the three different DEM resolutions (0.5 m, 1 m, 2 m) are plotted in Figure 12. The smoothing of the morphological change and associated transport rates is visible when moving from 0.5 m (red) to 2 m (green) DEM resolution. In our case, a DEM resolution of 0.5 m (or finer) appeared to be necessary.

3.7.2 The effect of survey frequency

The effect of survey frequency on derived morphological change (i.e. sequential erosion and deposition) is quantified in Figure 13a, where we compare the gross volume change (|erosion| + deposition) estimated for the 1st to the 6th August using two scans, with that estimated using additional scans within this period; 1st to 4th and 4th to 6th August (blue) and 1st to 3rd, 3rd to 4th and 4th to 6th (red). A c. 100% increase in the cumulated volume is observed if the scan frequency is increased from 2 to 4 scans over the same period and same number of events. A reduction in the number of flushing events between Lidar surveys leads to smaller bias in erosion-deposition volumes, <3'000 m^3 when 3 events occur between scans as compared to >6'000 m^3 when 22 events occur. Cumulative volume changes appear inversely proportional to scanning frequency and the number of events occurring between survey. This is the reason why the interval including the lowest number of flushing events (period 2 in Table 2: 3 events, 1 gravel, 2 sand) was used in this paper for the application of the morphological method.

Differences in morphological changes with survey frequency propagate into transport estimates through [3] and [7]. 1D transport rates for the same period 01.08-06.08, were calculated in Figure 13b for the same survey intervals. Generally, transport estimates tend to increase with survey frequency, suggesting sensitivity to the sequential erosion-deposition effect. However, an increase in survey frequency does not systematically lead to a higher transport rates (e.g. Figure 13b, green and blue curves between 300 m and 600 m) because it also depends on the timing of the survey with respect to the occurrence of compensating scour-fill events.

4. Discussion

The data collected and methods developed in this paper show how the morphological method can be applied in 1D and 2D over much larger spatial scales (kilometric) and at higher spatial resolution (centrimetric to metric) than has previously been the case, profiting from the progress made in both high resolution topographic data collection

and 2D hydraulic modelling. In theory, the 2D method may substantially reduce the uncertainty in estimating spatially-distributed transport fields in a modelling framework because erosion and deposition is determined directly, rather than inferred from, empirical, process relationships for entrainment and deposition.

This particular field setting, involving a water intake releasing water and sediment for known volumes and duration (Figure 2) and the ease of obtaining the necessary topographic data (i.e. Figure 1) allowed us to bypass some of the issues that have limited previous studies. These were often due to the problems associated with inundated areas (Lane, 2000), the unknown input of water and sediment into the system (e.g. Lane, 1997), and the unknown effective duration of flood events (e.g. Lane *et al.*, 1995). Whilst this case study was somewhat ideal, developments in both Structure from Motion photogrammetry (Westoby et al., 2012; Fonstad *et al.*, 2013; Woodget *et al.*, 2014; Carbonneau and Dietrich, 2017) and through water photogrammetry and image analysis (Westaway *et al.*, 2000, 2001; Lane *et al.* 2010; Dietrich, 2017), mean that the methodological limitations of previous applications of the 2D morphological method are being significantly reduced. Repeated high-resolution topographic data allowed determination of DEMs of difference (Figure 5) between each date of survey, and a cell-by-cell uncertainty analysis allowed us to apply a probabilistic thresholding to DEMs of Difference (Supporting Information S1).

The 2D approach (Figure 7) involved routing sediment through the network of braided channels based on a balance between flow driven shear stress (based on hydraulic simulations, Figure 3 a,b) and topography- or gravity-related shear stress (based on local cell slope). The no-negative transport condition is a more valuable parameter in the 2D case as it applies to every cell in the solution rather than individual sections (Figure 4c) and the condition was used in a Monte Carlo driven parameter sensitivity analysis. The method appears to be particularly dependent upon 1) the roughness and 2) the critical shear stress used to drive topographic forcing (Figures 8, 9; Table 3), which also emphasises the importance of the topographic forcing for sediment routing in braided rivers. The method was also able to reconstruct reasonable estimates of the sediment that needed to be supplied from upstream to minimise negative transport. Upstream supply was not a very sensitive parameter for the period that was investigated in this paper, but may become critical if net changes produced by a given event tend towards 0 or become negative (Lane *et al.*, 1995). Even with an optimised solution, a small percentage of negative transport remained, which is most likely a function of the different errors associated with the assumptions needed to realise the analysis (e.g. local DEM error, error related to the hydraulic model, application of a uniform grain size).

The 2D approach provided a spatially variable rate of transport in both downstream and the cross-stream directions (Figure 9). Compared to the 1D approach (Figure 6), the method considers only the morphological changes occurring within the inundated area (Figure 4c), which is likely to remove some of the impacts of residual noise present in the DEMs and which were not inundated during the flushing event. Furthermore, the spatial compensation of erosion and deposition was found to be substantial (0-90% of the volume per cross-section, 48% on average over the reach) and demonstrates the extent to which the 1D method's use of section net volumes of change is likely to produce incorrect bedload transport rate estimates, especially in more braided sections of a river (Figure 10). Process inference from section-integrated

bed-material transport overlooks the fact that sediment transport in braided rivers may vary significantly from one channel to the other, or within inundated cells of cross-section of a single channel (Ashmore, 1982, 1988, 1991a; Ferguson, 1993; Hoey and Sutherland, 1991). Nevertheless, in terms of the whole reach, most of the transport remained concentrated into one main anabranch during the studied flushing events, where 87 % of the total sediment mass was transferred. When combining the two largest anabranches, the proportion rose to 98 % (Figure 11a). It was only in braided zones that a significant proportion of the transport took place in secondary anabranches (up to 64% of the transport per cross-section, 15% on average over the reach), and the proportion of transport in secondary anabranches tended to increase with braiding intensity (Figure 11b). This suggests that braided channels are able to redistribute bedload, and each anabranch may behave like an individual single-thread channel (potentially with its own spatially compensating deposition and erosion) when the braiding intensity increases (e.g. Ashmore, 1991a; Ferguson, 1993).

Some broad challenges remain in the field application of the morphological method. First, there is the determination of the competent flow duration (t_c in [3] and [7]), that is the length of time over which the morphological changes are assumed to occur (Lane *et al.*, 1995). This is a particular issue in gravel-bed rivers as transport tends to be threshold-dominated such that the competent flow duration may be much less than the time between survey. In this application, the flushing duration appears to be a reasonable estimate of actual competent flow duration, because transport starts and stops abruptly as the intake gate opens and closes. In other applications, where t_c is less well known, underestimation of transport rates may result. Combining repeated topographic data acquisition with, for example, seismic sensors (e.g. Burtin *et al.*, 2011) may provide constraints on values of t_c. Second, we could only partially exclude the problem of 'travelling bedload' (Piton and Recking, 2017), that is the extent to which there can be sediment throughput within an event without morphological expression. This depends on the duration of transport competence as compared with the downstream length of survey: with smaller durations of competence and longer survey lengths, there is greater probability that there is no sediment throughput during an event. Under the assumption that the supplied sediment was correctly specified, the 1D results allowed us to identify the maximum possible throughput of sediment, that is the minimum estimated transport rate within the reach. One interesting approach here would be to support this method with some particle tracking to quantify typical competence duration and travelling distance (e.g. Hassan *et al.*, 2013), and hence to identify the survey lengths needed to avoid sediment throughput for a given competent flow duration. Third, we showed the effect of increasing DEM resolution on transport rate estimates, where more topographic complexity is captured as the data spatial resolution increases (Figure 13). The resolution of topographic data needed to apply the morphological method should be carefully considered and should reflect the scale of river bathymetry under consideration (Lane *et al.*, 1994; Lane, 1998a; Vericat *et al.*, 2017). Finally, the results confirmed the underestimation of cumulated volumes of change that can arise, notably due to sequential erosion and deposition (or *vice versa*) through time between survey dates. This may be within an individual sediment transport event, or for a sequence of events, and these clearly propagate into transport rate estimates (Figure 13). In this paper, cumulative volume change appears to be inversely proportional to the duration between topographic surveys, which is in line with findings from other studies. In a flume study of a braiding river, Lindsay and Ashmore (2002) reported that an 80 % increase in the volume of change followed a

reduction in the time between survey of 50%. Lane *et al.* (1994), in a field experiment, observed a 122% increase in river bed volume changes when the duration between surveys was reduced by 56%. In this study, we observed a 100% increase in volume change when reducing the duration between topographic surveys by 80%, which is a lower magnitude for the sequential erosion and deposition effect that reported in previous studies. Measured morphological change (and derived transport rates) should increase as survey interval decreases to the point at which, theoretically, survey frequency covers the motion of each individual particle. Such frequency of survey is unfeasible and this represents a fundamental limitation of the morphological method. However, the problem may be minimized by making sure that resurvey of a stream matches the rate at which it is changing. Lane et al. (1994, 1996), for instance, showed how collected DEMs in a glacially-fed braided stream at the morning low flow and the late afternoon high flow captured a significant amount of sequential erosion and deposition effects.

5. Conclusions

More than twenty years since its first application in 2D (Lane *et al.*, 1995), this paper revisits the 1D and 2D morphological method for bed-material transport estimation. Aided by progress in both high-resolution topographic data collection and hydraulic modelling, we could apply the method to a 1600 m x 300 m Alpine braided river reach, and collect topographic data at a centimetric resolution within a few minutes. In comparison, Lane *et al.* (1995) needed several hours to survey a much smaller surface (20 m x 8 m) at lower spatial resolution (decimetric to metric), which did not allow the full investigation of the spatial distribution of transport rates within a network of braided anabranches. We applied the method to an Alpine braided river 'laboratory', where flow abstraction and flushing of a water intake allowed us to acquire high resolution topographic data using terrestrial laser scanning and provided access to water and sediment supply data when the water intake was flushed yielding low magnitude flood events. While the application of the morphological method in 1D only gave information on the downstream variability in transport rates along the reach, its application in 2D provided information on the cross-channel variation in the contribution of bed-material erosion and deposition to bed-material transport. This revealed a substantial spatial compensation of erosion and deposition within a section associated with application of the 1D method, to a degree related to braiding intensity. We also found that even if a great majority of the transport took place in one anabranch, a significant proportion of the transport occurred in the secondary anabranches once the river started braiding, and that proportion tended to increase with braiding intensity, showing the ability of the river to redistribute the sediment in the network of braided channels..

The application of the morphological method in two dimensions is likely to bring new insights into river geomorphology in the immediate future because it provides spatially-distributed estimates of bed-material transport. Although these are time-integrated, are dependent on DEM spatial resolution and survey frequency, and are subject to sequential erosion-deposition through time between survey dates and 'travelling bedload' effects, they may likely provide additional means to develop relationships between transport and local hydraulic forcing (e.g. shear stress) to improve sediment transport predictions (e.g. Rickenmann *et al.*, 1991), and to improve our understanding of complex fluvial processes such as braiding (e.g. Vericat *et al.*, 2017). This process will be aided by the suite of new methods that are increasing the extent to which high

resolution topographic data of the river bed can be accurately acquired, including in stream bathymetry with progress with unmanned airborne vehicles (e.g. Woodget *et al.*, 2014; Dietrich, 2017), green Lidar (i.e. Kinzel *et al.*, 2013) and acoustic Doppler survey (i.e. Rennie and Church, 2010).

6. Acknowledgements

7. References

Anderson S, Pitlick, J. 2014. Using repeat lidar to estimate sediment transport in a steep stream. *Journal of Geophysical Research: Earth Surface*, *119*(3), 621-643.

Ashmore PE. 1982. Laboratory modelling of gravel braided stream morphology. *Earth Surface Processes and Landforms*, 7, 201-225.

Ashmore PE. 1988. Bedload transport in braided gravel-bed stream models. *Earth Surface Processes and Landforms*, 13, 677-695.

Ashmore PE. 1991. How do gravel-bed rivers braid? *Canadian Journal of Earth Science,* 28 (3), 326-341.

Ashmore PE and Church M. 1998. Sediment transport and river morphology: a paradigm for study. In R. D. Hey, J. C. Bathurst and C. R. Thorne (eds). *Gravel-bed Rivers in the Environment.* Wiley : Chichester, 115–148.

Ashworth PJ. and Ferguson RI. 1986. Interrelationships of Channel Processes, Changes, and Sediments in a Proglacial Braided River. *Geografiska Annaler, Series A, Physical Geography*, 68(4), 361-371.

Bakker M, Costa A, Silva, TA, Stutenbecker L, Girardclos S, Loizeau, JL, Molnar P, Schlunegger F. and Lane SN. 2018. Combined Flow Abstraction and Climate Change Impacts on an Aggrading Alpine River. Water Resour. Res. 54, 223-42

Bakker M, Lane, SN. 2016. Archival photogrammetric analysis of river–floodplain systems using Structure from Motion (SfM) methods. *Earth Surface Processes and Landforms*, *42*(8), 1274-1286.

Bates PD, Lane, SN, Ferguson RI. (Eds.). 2005. *Computational fluid dynamics: applications in environmental hydraulics*. John Wiley & Sons.

Bendegom LV. van. 1947. Some considerations on river morphology and river improvement, De Ingenieur vol. 59–4, pp. B1–11. *Dutch. English translation: Nat. Res. Council of Canada, Tech. Transi*, *1054*, 1963.

Beven K, Binley A. 1992. The future of distributed models: model calibration and uncertainty prediction. *Hydrological processes*, *6*(3), 279-298.

Bezinge A, Clark MJ, Gurnell AM, Warburton J. 1989. The management of sediment transported by glacial melt-water streams and its significance for the estimation of sediment yield. Sion. *Annals of Glaciology*, 13, 1-5.

Bohorquez P, Darby SE. 2008. The use of one-and two-dimensional hydraulic modelling to reconstruct a glacial outburst flood in a steep Alpine valley. *Journal of hydrology*, *361*(3-4), 240-261.

Brasington J, Rumsby BT, McVey RA. 2000. Monitoring and modelling morphological change in a braided gravel-bed river using high resolution GPS-based survey. *Earth Surface Processes and Landforms*, 25, 973-990.

Brasington J, Langham J, Rumsby B. 2003. Methodological sensitivity of morphometric estimates of coarse fluvial sediment transport. *Geomorphology*, *53*(3), 299-316.

Brasington J, Vericat D., Rychkov I. 2012. Modeling river bed morphology roughness and surface sedimentology using high resolution terrestrial laser scanning. *Water Ressources Research*, 48 (11).

Burtin, A., Cattin, R., Bollinger, L., Vergne, J., Steer, P., Robert, A., ... & Tiberi, C. 2011. Towards the hydrologic and bed load monitoring from high-frequency seismic noise in a braided river: The "torrent de St Pierre", French Alps. *Journal of hydrology*, *408*(1-2), 43-53.

Carbonneau PE, Lane SN, Bergeron NE. 2004. Catchment-scale mapping of surface grain size in gravel bed rivers using airborne digital imagery. *Water resources research*, *40*(7).

Carbonneau PE, Dietrich, JT .2017. Cost-effective non-metric photogrammetry from consumer-grade sUAS: implications for direct georeferencing of structure from motion photogrammetry. *Earth Surf. Process. Landforms*, 42: 473–486.

Carling PA, Reader NA. 1982. Structure, composition and bulk properties of upland stream gravels. *Earth Surface Processes and Landforms*, 7(4), 349-365.

Chandler J, Ashmore PE, Paola C, Gooch M, Varkaris F. 2002. Monitoring river channel change using terrestial oblique digital imagery and automated digital photogrammetry. *Annals of the Association of American Geographers*, 92(4), 631-644.

Church M. 2006. Bed material transport and the morphology of alluvial river channels. *Annu. Rev. Earth Planet. Sci.*, *34*, 325-354.

Dietrich JT. 2017 Bathymetric Structure-from-Motion: extracting shallow stream bathymetry from multi-view stereo photogrammetry. *Earth Surf. Process. Landforms*, 42: 355–364. doi: 10.1002/esp.4060.

Engelund F. 1974. Flow and bed topography in channel bends. *Journal of the Hydraulics Division*, *100*(Proc. Paper 10963).

Exner FM. 1925. Uber die wechselwirkung zwischen wasser und geschiebe in flussen. *Akad. Wiss. Wien Math. Naturwiss. Klasse*, *134*(2a), 165-204.

Faeh R, Mueller R, Rousselot P, Vetsch D, Volz C, Vonwiller, L, Veprek R, Farshi D. 2011. *System Manuals of BASEMENT,* Version 2.1. ETH Zürich : Laboratory of Hydraulics, Glaciology and Hydrology (VAW). Disponible sur http://www.basement.ethz.ch/docs (consulté le 22.04.2013).

Ferguson RI. 1993. Understanding braiding processes in gravel-bed rivers: process and unsolved problems. *Geological Society of London – Special Publications,* 75, 73-87.

Ferguson RI. 2010. Time to abandon the Manning equation?. *Earth Surface Processes and Landforms*, *35*(15), 1873-1876.

Fonstad MA, Dietrich JT, Courville BC, Jensen JL, Carbonneau, PE. 2013. Topographic structure from motion: a new development in photogrammetric measurement. *Earth Surface Processes and Landforms*, *38*(4), 421-430.

Fuller IC, Large, ARG, Charlton ME, Heritage GL, Milan DJ. 2003. Reach-scale sediment transfers: an evaluation of two morphological budgeting approaches. *Earth Surface Processes and Landforms*, 28, 889-903.

Gabbud C, Micheletti N, Lane SN. 2015. Lidar measurement of surface melt for a temperate Alpine glacier at the seasonal and hourly scales. *Journal of Glaciology*, *61*(229), 963-974.

Haff PK. 1996. Limitations on Predictive Modeling in Geomorphology. In Bruce L. Rhoads and Colin E. Thorn, The Scientific Nature of Geomorphology, Wiley, Chichester, 337-58.

Hardy RJ, Lane SN, Lawless MR, Best JL, Elliott L, Ingham DB. .2005. Development and testing of a numerical code for treatment of complex river channel topography in three-dimensional CFD models with structured grids. *Journal of Hydraulic Research*, *43*(5), 468-480.

Hassan MA, Voepel H, Schumer R, Parker G, Fraccarollo L. 2013. Displacement characteristics of coarse fluvial bed sediment. *Journal of Geophysical Research: Earth Surface*, *118*(1), 155-165.

Heritage G. and Hetherington D. 2007. Towards a protocol for laser scanning in fluvial geomorphology. *Earth Surface Processes and Landforms,* 32, 66-74.

Hoey TB, Sutherland AJ. 1991. Channel morphology and bedload pulses in braided rivers: a laboratory study. *Earth Surface Processes and Landforms*, 16, 447-462.

Ikeda H. 1989. Sedimentary controls on channel migration and origin of point bars in sand–bedded meandering rivers. *River meandering*, 51-68.

Ingham DB, Ma L. 2005. Fundamental equations for CFD in river flow simulations. In: Bates PD, Lane SN. and Ferguson RI. (eds) Computational fluid dynamics applications in environmental hydraulics. Chichester, UK: John Wiley & Sons, pp. 19 – 49.

Javernick L, Brasington J, Caruso B. 2014. Modeling the topography of shallow braided rivers using Structure-from-Motion photogrammetry. *Geomorphology*, *213*, 166-182.

Julien PY. 2002. *River Mechanics.* Cambridge University Press, Cambridge, 456pp.

Kinzel PJ, Legleiter CJ, Nelson JM. 2013. Mapping river bathymetry with a small footprint green LiDAR: Applications and challenges. *JAWRA Journal of the American Water Resources Association*, *49*(1), 183-204.

Lane SN. 1997. The reconstruction of bed material yield and supply histories in gravel-bed streams. *Catena*, *30*(2-3), 183-196.

Lane SN. 1998a. The use of digital terrain modelling in the understanding of dynamic river channel systems. In Lane, S. N., Richards, K. S and Chandler, J. H. (eds.) *Landform monitoring, modelling and analysis.* Chichester : John Wiley and Sons, 454p.

Lane SN. 1998b. Hydraulic modelling in hydrology and geomorphology: a review of high resolution approaches. *Hydrological Processes*, *12*(8), 1131-1150.

Lane SN. 2000. The Measurement of River Channel Morphology. *Photogrammetric Record,* 16, 937-961.

Lane SN. 2005. Roughness : time for a re-evaluation. *Earth Surface Processes and Landforms*, 30 (2), 251-253.

Lane SN, Richards KS, Chandler JH. 1994. Development in monitoring and modelling small-scale river bed topography. *Earth Surface Processes and Landforms*, 19 (4), 349-368.

Lane SN, Richards KS, Chandler JH. 1995. Morphological estimation of the time-integrated bedload transport rate. *Water Resources Research,* 761-772.

Lane SN, Richards KS, Chandler JH. 1996. Discharge and sediment supply controls on erosion and deposition in a dynamic alluvial channel. *Geomorphology*, 15, 1-15

Lane SN, Bradbrook, KF, Richards KS, Biron PA, Roy AG. 1999. The application of computational fluid dynamics to natural river channels: three-dimensional versus two-dimensional approaches. *Geomorphology*, *29*(1-2), 1-20.

Lane SN, Westaway RM, Hicks MD. 2003. Estimation of erosion and deposition volumes in a large, gravel-bed, braided river using synoptic remote sensing. *Earth Surface Processes and Landforms*, 28, 249-271.

Lane SN, Hardy RJ, Ferguson RI, Parsons DR. 2005. A framework for model verification and validation of C2005FD schemes in natural open channel flows. In P. D. Bates, S. N. Lane and R. I. Ferguson (Eds). *Computational Fluid Dynamics : Application in Environnemental Hydraulics* (pp. 147-168). Chichester : John Wileys and Sons.

Lane SN, Bakker M, Gabbud C, Micheletti N, Saugy JN. 2017. Sediment export, transient landscape response and catchment-scale connectivity following rapid climate warming and Alpine glacier recession. *Geomorphology*, *277*, 210-227.

Lindsay JB, Ashmore PE. 2002. The effects of survey frequency on estimates of scour and fill in a braided river model. *Earth Surface Processes and Landforms*, *27*(1), 27-43.

Meyer-Peter E, Müller R. 1948. Formulas for bed-load transport. In *IAHSR 2nd meeting, Stockholm, appendix 2*. IAHR.

Milan DJ, Heritage GL, Hetherington D. 2007. Application of a 3D laser scanner in the assessment of erosion and deposition volumes and channel change in a proglacial river. *Earth Surface Processes and Landforms,* 32, 1657-1674.

Mosselman E. 2005. Basic equations for sediment transport in CFD for fluvial morphodynamics. *Computational fluid dynamics: applications in environmental hydraulics*, 71-89.

Nelson JM, Smith JD. 1989. Flow in meandering channels with natural topography. *River meandering*, 69-102.

Newson M. 1980. The geomorphological effectiveness of floods—a contribution stimulated by two recent events in mid-wales. Earth Surf. Process., 5: 1-1.

Nicholas AP. 2003. Investigation of spatially distributed braided river flows using a two-dimensional hydraulic model. *Earth Surface Processes and Landforms*, *28*(6), 655-674.

Nicholas AP, Ashworth PJ, Kirkby MJ, Macklin MG, Murray T. 1995. Sediment slugs: large-scale fluctuations in fluvial sediment transport rates and storage volumes. *Progress in physical geography*, *19*(4), 500-519.

Nicholas AP, Sambrook Smith GH. 1999. Numerical simulation of three-dimensional flow hydraulics in a braided channel. *Hydrological Processes*, *13*(6), 913-929.

Nitsche M, Rickenmann D, Turowski JM, Badoux A, Kirchner JW. 2011. Evaluation of bedload transport predictions using flow resistance equations to account for macro-roughness in steep mountain streams. *Water Resources Research*, *47*(8).

Picco L, Mao L, Cavalli M, Buzzi E, Rainato R, Lenzi MA. 2013. Evaluating short-term morphological changes in a gravel-bed braided river using terrestrial laser scanner. *Geomorphology*, *201*, 323-334.

Piton G, Recking A. 2017. The concept of travelling bedload and its consequences for bedload computation in mountain streams. *Earth Surf. Process. Landforms*, 42: 1505–1519.

Rennie CD, Church M. 2010. Mapping spatial distributions and uncertainty of water and sediment flux in a large gravel bed river reach using an acoustic Doppler current profiler. *Journal of Geophysical Research: Earth Surface*, *115*(F3).

Rickenmann D. 1991. Hyperconcentrated flow and sediment transport at steep slopes. *Journal of hydraulic engineering*, *117*(11), 1419-1439.

Struiksma N, Crosato A. 1989. *Analysis of a 2-D Bed Topography Model for Rivers* (pp. 153-180). American Geophysical Union.

Tal M, Paola C. 2010. Effects of vegetation on channel morphodynamics: results and insights from laboratory experiments. Earth Surface Processes and Landforms, 35, 1014–1028.

Vericat D, Wheaton JM, Brasington J. 2017. Revisiting the Morphological Approach: Opportunities and Challenges with Repeat High-Resolution Topography. *Gravel-Bed Rivers: Process and Disasters*, 121.

Warburton J. 1992. Observations of Bedload Transport and Channel Bed Changes in a Proglacial Mountain Stream. *Arctic and Alpine Research*, 3, 195-203.

Westaway RM, Lane SN, Hicks DM. 2000. The development of an automated correction procedure for digital photogrammetry for the study of wide, shallow gravel-bed rivers. *Earth Surface Processes and Landforms,* 25, 209-226.

Westaway RM, Lane SN, Hicks DM. 2003. Remote survey of large-scale braided, gravel-bed rivers using digital photogrammetry and image analysis. *International Journal of Remote Sensing,* 24 (4), 795-815.

Westoby MJ, Brasington J, Glasser NF, Hambrey MJ, Reynolds JM. 2012. 'Structure-from-Motion'photogrammetry: A low-cost, effective tool for geoscience applications. *Geomorphology*, *179*, 300-314.

Wheaton JM, Brasington J, Darby SE, David AS. 2010. Accounting for uncertainty in DEMs from repeat topographic surveys: improved sediment budgets. *Earth Surface Processes and Landforms,* 35, 136-156.

Wheaton JM, Brasington J, Darby SE, Kasprak A, David AS, Vericat D. 2013. Morphodynamic signatures of braiding mechanisms as expressed through change sediment storage in a gravel-bed river. *Journal of Geophysical Research: Earth Surface,* 118, 759-779.

Williams RD, Brasington J, Vericat D, Hicks DM. 2014. Hyperscale terrain modelling of braided rivers: fusing mobile terrestrial laser scanning and optical bathymetric mapping. *Earth Surface Processes and Landforms,* 39: 167–183.

Williams RD, Brasington J, Hicks DM. 2016. Numerical modelling of braided river morphodynamics: Review and future challenges. *Geography Compass*, *10*(3), 102-127.

Wolman MG. 1954. A method of sampling coarse river-bed material. *EOS, Transactions American Geophysical Union*, *35*(6), 951-956.

Woodget AS, Carbonneau PE, Visser F, Maddock IP. 2014. Quantifying submerged fluvial topography using hyperspatial resolution UAS imagery and structure from motion photogrammetry, *Earth Surf. Process. Landforms*, 40, 47–64

Wright NG. 2005. Introduction to numerical methods for fluid flow. In P. D. Bates, S. N. Lane and R. I. Ferguson (Eds). *Computational Fluid Dynamics : Application in Environnemental Hydraulics* (pp. 147-168). Chichester : John Wileys and Sons.

Zanoni L, Gurnell AM, Drake N, Surian N. 2008. Island dynamics in a braided river from analysis of historical maps and air photographs. *River Research and Applications*, 24, 1141–1159.

Zhang Z. 1994. Iterative point matching for registration of free-form curves and surfaces. *International journal of computer vision*, *13*(2), 119-152.

Table 1. Scan and registration details.

Scan day / time	Duration [min]	Number of points	Point per square meter [pts/m^2]	Std. Dev. of residuals after registration (reference 1st August) [m]
01 August / 8am	4.3	1'643'508	5.57	± 0.000
03 August / 4pm	8.1	3'098'416	12.39	± 0.035
04 August / 12pm	8.3	3'093'024	12.37	± 0.039
06 August / 2pm	8.4	3'151'680	12.61	± 0.040

Table 2. Occurrence of flushing events, type (S = sand-dominated, G = gravel-dominated), competent flow duration [min], maximum discharge [m^{3}s^{-1}], volume [m^3] and mass [kg] of sediment released by each flushing event. Period intervals are determined by the Lidar surveys (Table 1). Input of sediment and competent flow duration for each period were determined by cumulating the sediment input and duration of each individual flushing event contained within that interval. Maximum discharge was defined as the highest discharge estimated for each scanning interval. Details of flushing events are available in Supporting Information S2.

	Period	No. flushing events	Type	t_c [min]	Q_{max} [m^{3}s^{-1}]	Sed. input volume [m^3]	Sed. input mass [kg]
1.	01-03	10	8S / 2G	420	1.19	356 ± 108	462 ± 143
2.	03-04	3	2S / 1G	180	1.35	164 ± 27	213 ± 43
3.	04-06	9	7S / 2G	360	1.53	349 ± 57	453 ± 77
4.	01-04	13	10S / 3G	600	1.35	520 ± 135	606 ± 187
5.	01-06	22	17S / 5G	960	1.53	869 ± 110	1128 ± 263

Table 3. Parameter ranges use in the GLUE estimation for the survey period 3rd to 4th of August (period 2 in Table 2).

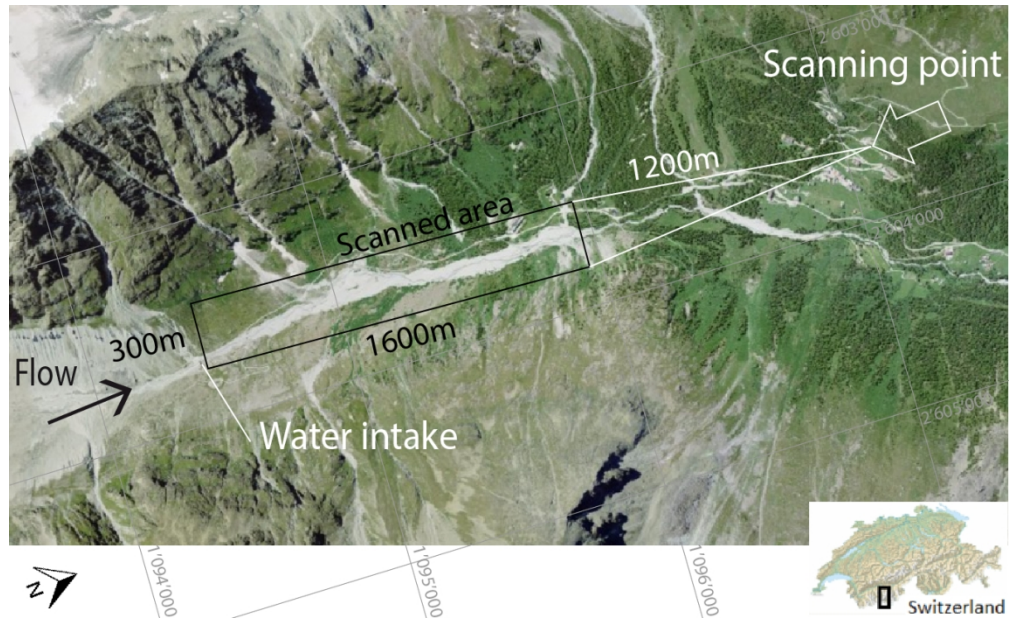| Parameter	Minimum value	Maximum value	Comments
Upstream sediment supply rate (m^3)	0	250	Envelopes the estimated volume of sediment released in the sequences of flushing events (Table 2). Distributed equally across the wet model inlet cells.
Angle of repose (°)	17.5	45	Envelopes sin(30°) angle of repose.
Critical shear stress (Nm^{-2})	0	100	Zero corresponds to no topographic correction and 100 a grain size of c. 128 mm (after Julien, 2002).
Manning's n	0.01	0.1	Envelopes a range of possible n values

Figure 1. Study site with the scanned area, the water intake and the scanning point (© Swisstopo for satellite images and © Wikipédia for the map of Switzerland, coordinates are in CH1903+ system).

Figure 2. Discharge released into the study reach during the survey period, which provided flushing magnitude and duration, and enabled distinction to be made between flushing of the gravel and the sand traps, and therefore the amount of sediment released in the system during each event (Supporting Information S2) and each survey interval.

Figure 3. Simulated water depths (a) and flow velocities (b) for a braided river section (400 m - 900 m); period: 3rd to 4th of August (period 2 in Table 2). Flow direction is from left to right.

Figure 4. Illustration of the application of the 1D and 2D morphological method.

Figure 5. DEM of difference with a grid resolution of 0.5 m for the period 01th to 06th of August (period 5 in Table 2).

Figure 6. Downstream variability in 1D bed-material transport rate [kg/s] based on the morphological changes measured for the period 3rd to 4th of August (period 2 in Table 2). Note that a 20 m moving mean was applied in the figure to 1D transport rate for visualisation purposes.

Figure 7. Mean (black) and standard deviation (red) of 2D transport sensitivity analysis: (1) the upstream sediment supply [m^3] (top left), (2) the angle of repose [°] (top right), (3) the critical shear stress [Nm^{-2}] (bottom left) and (4) Manning's n [-] (bottom right) for the period 3rd to 4th of August (period 2 in Table 2).

Figure 8. 2D bed-material transport predictions for (a) the case of zero sediment supply and topographic forcing; (b) and 160 m^3 upstream supply and a critical shear stress of 40 Nm^{-2} for the period 3rd to 4th of August (period 2 in Table 2).

Figure 9. 2D transport rates for the period 3rd to 4th of August (period 2 in Table 2). River flows from top to bottom and the river reach is split in two figures for visualization purpose. Discharge is 1.35 m^3/s, upstream sediment supply is 160 m^3, critical shear stress is 40 Nm^{-2}, Manning's n is 0.07 and the angle of repose is 31° (values obtained though model optimization).

Figure 10. Difference between gross change and net change per cross section for the period 3rd to 4th of August (period 2 in Table 2), quantifying the relative volume locally unaccounted when using a 1D morphological approach. Positive correlation with number of anabranches per cross section (r = 0.43, p < 0.05). Note that a 20 m moving mean was applied in the figure to the unaccounted volume and number of anabranches for visualisation purposes.

Figure 11. a) contribution of each anabranch to the total transport rate for period 3rd to 4th of August (period 2 in Table 2); b) Proportion of transport taking place in secondary anabranches [%] is positively correlated with the number of anabranch per cross-section (r = 0.52, p < 0.05). Note that a 20 m moving mean was applied in the figure on the different curves for visualisation purposes.

Figure 12. 1D transport rates calculated for the period 3rd to 4th of August (period 2 in Table 2) with DEM resolutions of 0.5 m, 1 m and 2 m. Note that a 20 m moving mean was applied tin the figure on the different curves for visualisation purposes.

Figure 13. a) Effect of scan frequency and number of flushing events upon the gross volume change and b) Upon 1D transport rates. Overall, the greater the number of flushing events, the more likely the compensating scour-fill effect and the smaller the derived morphological changes and transport rates. Note that a 20 m moving mean was applied tin the figure on the different curves for visualisation purposes.

Figure 1. Study site with the scanned area, the water intake and the scanning point (© Swisstopo for satellite images and © Wikipédia for the map of Switzerland, coordinates are in CH1903+ system).
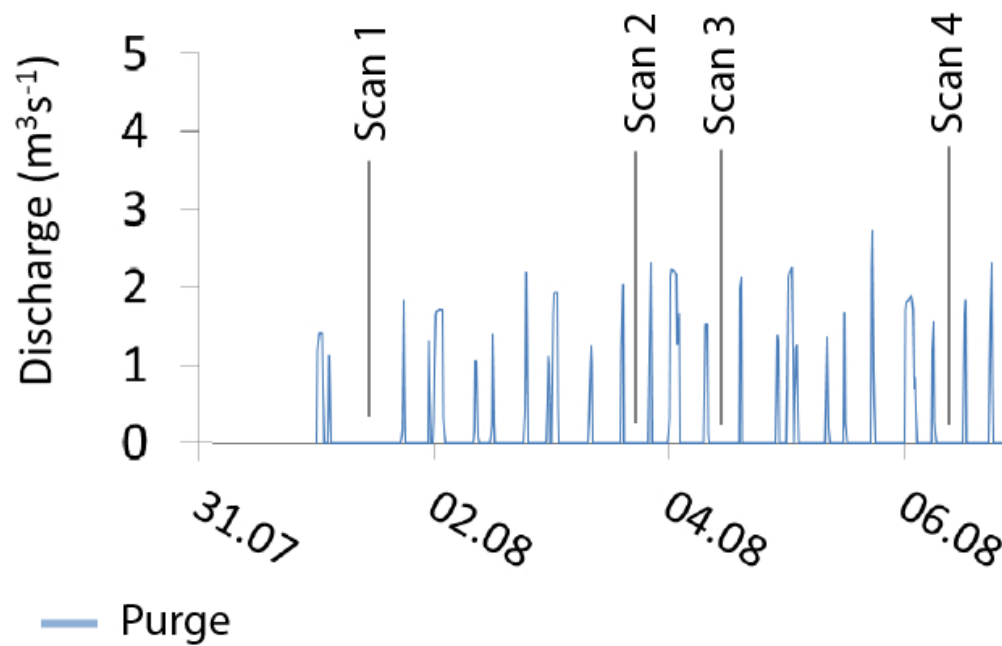
Figure 2. Discharge released into the study reach during the survey period, which provided flushing magnitude and duration, and enabled distinction to be made between flushing of the gravel and the sand traps, and therefore the amount of sediment released in the system during each event (Supporting Information S2) and each survey interval.

1
2
3
4
5
6
7
8
9
10
11
12
13
14
15
16
17
18
19
20
21
22
23
24
25
26
27
28
29
30
31
32
33
34
35
36
37
38
39
40
41
42
43
44
45
46
47
48
49
50
51
52
53
54
55
56
57
58
59
60
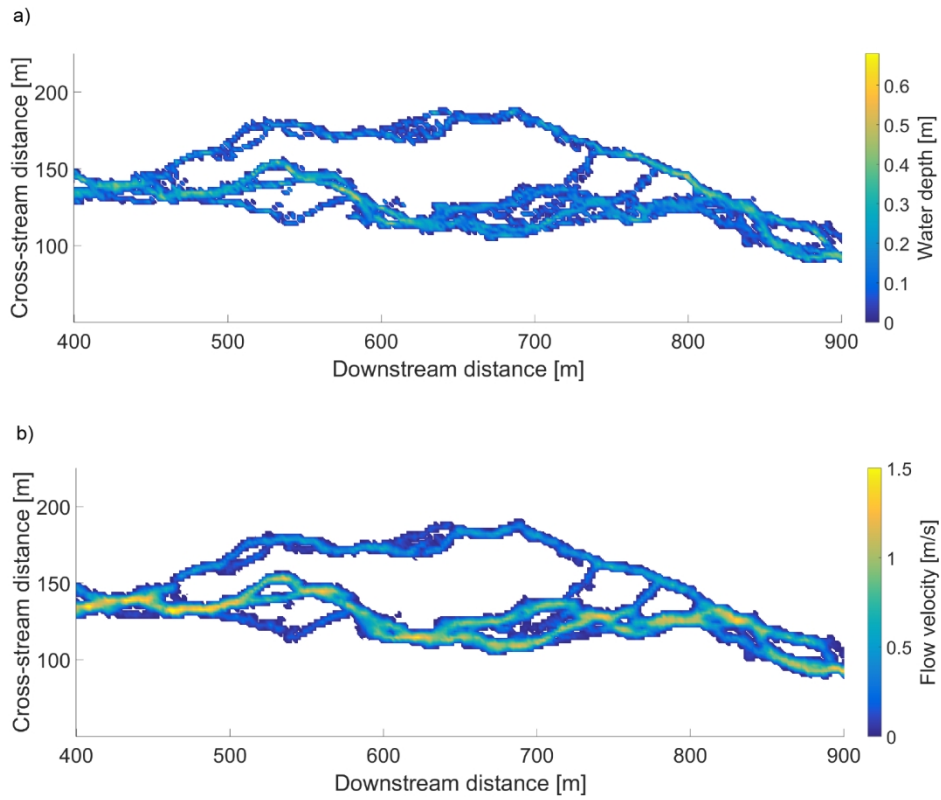
Figure 3. Simulated water depths (a) and flow velocities (b) for a braided river section (400 m - 900 m); period: 3rd to 4th of August (period 2 in Table 2). Flow direction is from left to right.
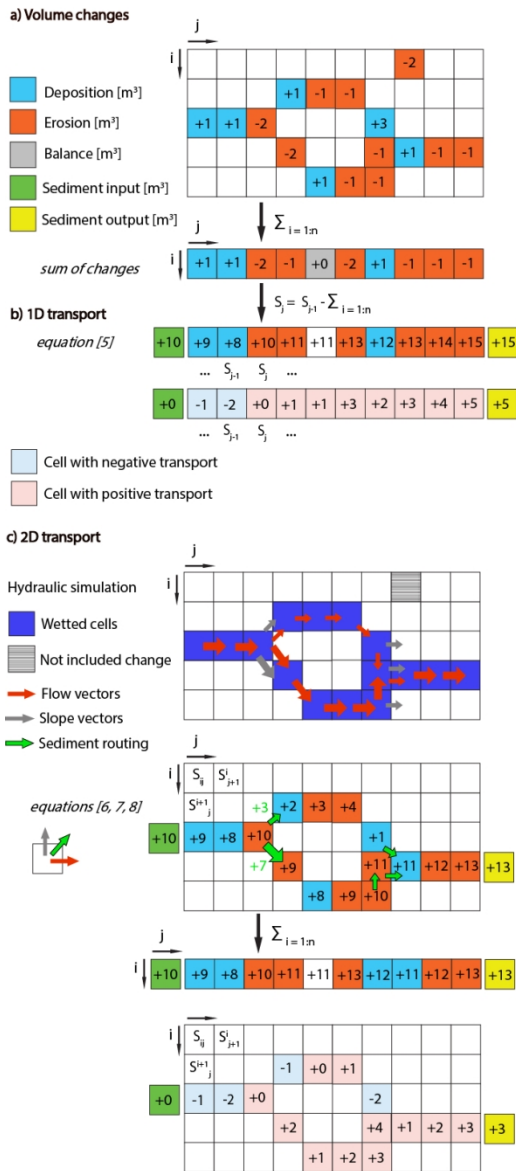
Figure 4. Illustration of the application of the 1D and 2D morphological method.

1
2
3
4
5
6
7
8
9
10
11
12
13
14
15
16
17
18
19
20
21
22
23
24
25
26
27
28
29
30
31
32
33
34
35
36
37
38
39
40
41
42
43
44
45
46
47
48
49
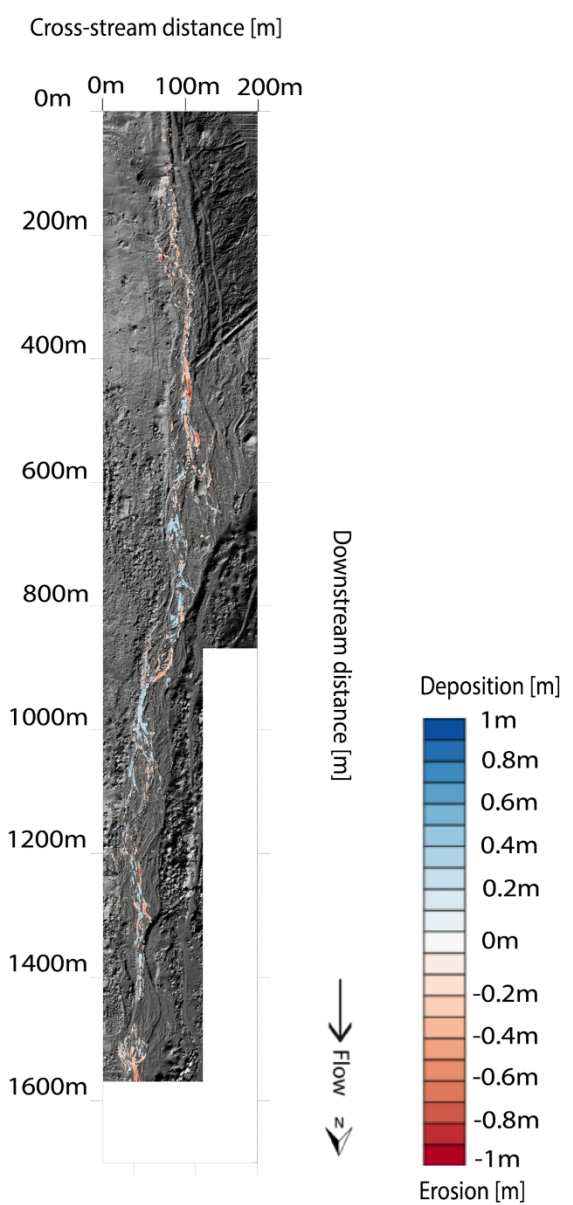50
51
52
53
54
55
56
57
58
59
60

Figure 5. DEM of difference with a grid resolution of 0.5 m for the period 01th to 06th of August (period 5 in Table 2).
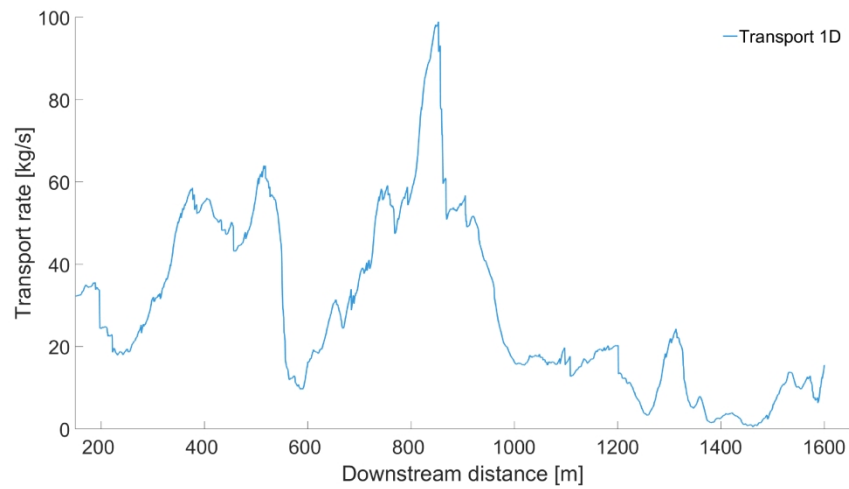
Figure 6. Downstream variability in 1D bed-material transport rate [kg/s] based on the morphological changes measured for the period 3rd to 4th of August (period 2 in Table 2). Note that a 20 m moving mean was applied in the figure to 1D transport rate for visualisation purposes.
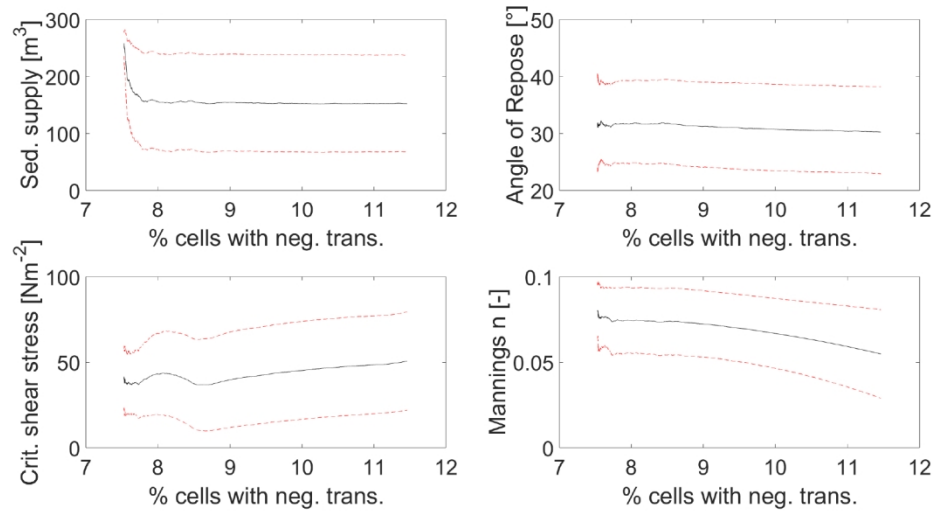
1
2
3
4
5
6
7
8
9
10
11
12
13
14
15
16
17
18
19
20
21
22
23
24
25
26
27

Figure 7. Mean (black) and standard deviation (red) of 2D transport sensitivity analysis: (1) the upstream sediment supply [m3] (top left), (2) the angle of repose [°] (top right), (3) the critical shear stress [Nm-2] (bottom left) and (4) Manning's n [-] (bottom right) for the period 3rd to 4th of August (period 2 in Table 2).

28
29
30
31
32
33
34
35
36
37
38
39
40
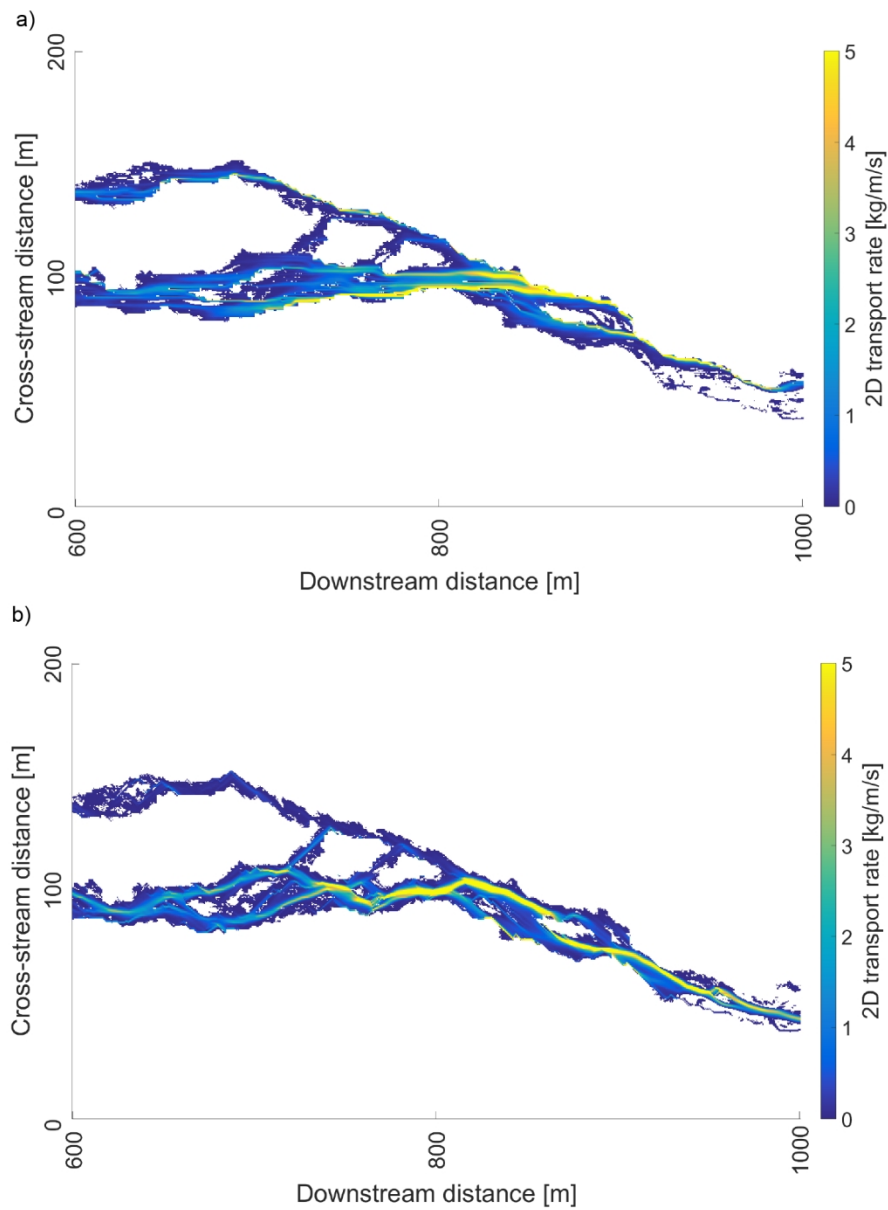41
42
43
44
45
46
47
48
49
50
51
52
53
54
55
56
57
58
59
60

Figure 8. 2D bed material transport predictions for (a) the case of zero sediment supply and topographic forcing; (b) and 160 m3 upstream supply and a critical shear stress of 40 Nm-2 for for the period 3rd to 4th of August (period 2 in Table 2).
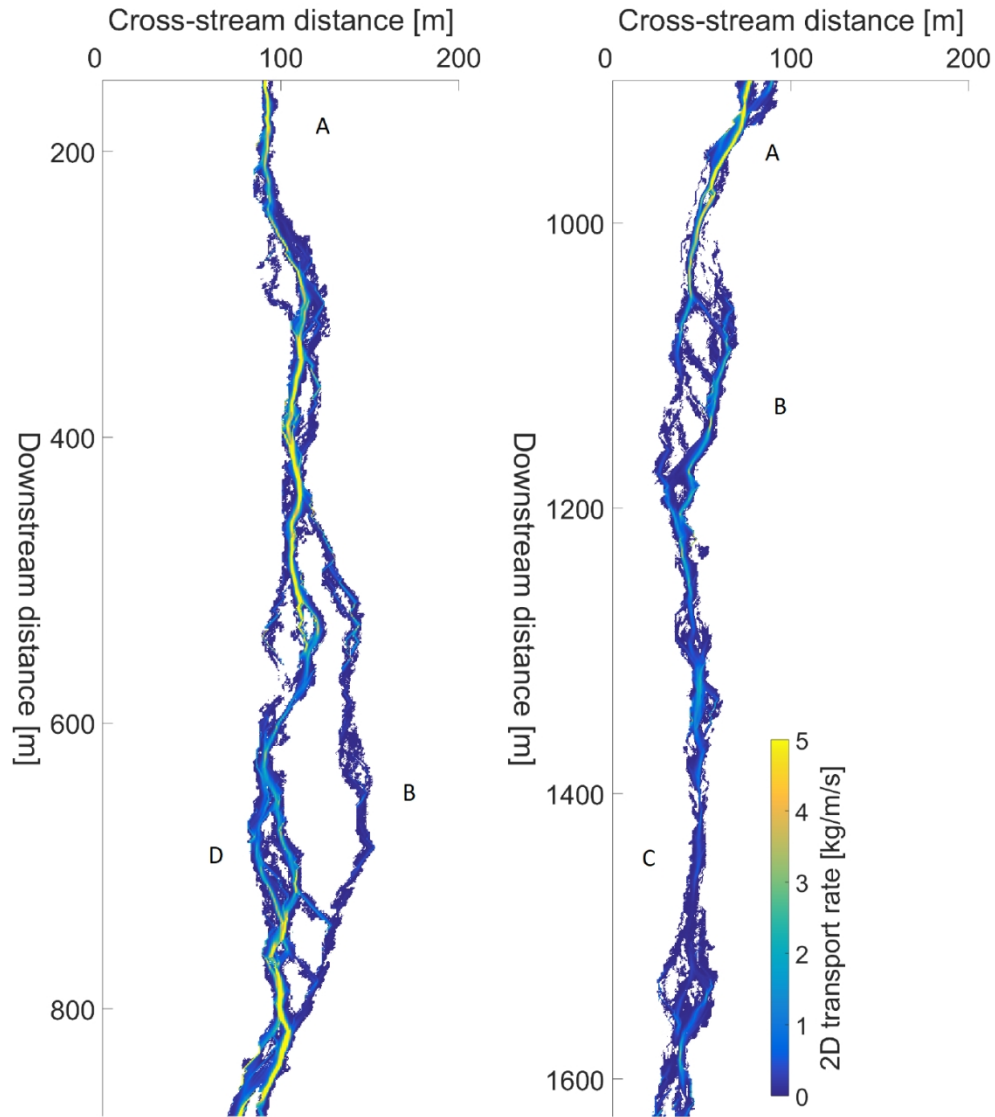
Figure 9. 2D transport rates for the period 3rd to 4th of August (period 2 in Table 2). River flows from top to bottom and the river reach is split in two figures for visualization purpose. Discharge is 1.35 m3/s, upstream sediment supply is 160 m3, critical shear stress is 40 Nm-2, Manning's n is 0.07 and the angle of repose is 31° (values obtained though model optimization).
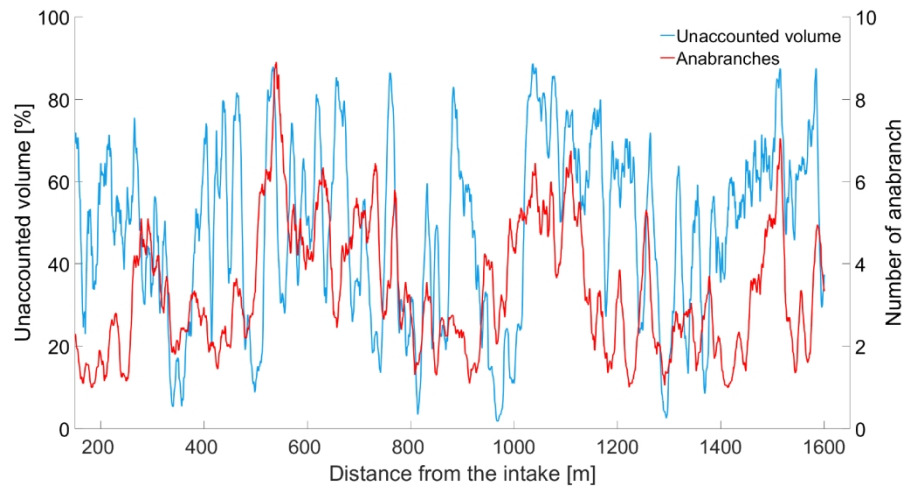
Figure 10. Difference between gross change and net change per cross section for the period 3rd to 4th of August (period 2 in Table 2), quantifying the relative volume locally unaccounted when using a 1D morphological approach. Note that a 20 m moving mean was applied to the unaccounted volume and number of anabranches for visualisation purposes.

1
2
3
4
5
6
7
8
9
10
11
12
13
14
15
16
17
18
19
20
21
22
23
24
25
26
27
28
29
30
31
32
33
34
35
36
37
38
39
40
41
42
43
44
45
46
47
48
49
50
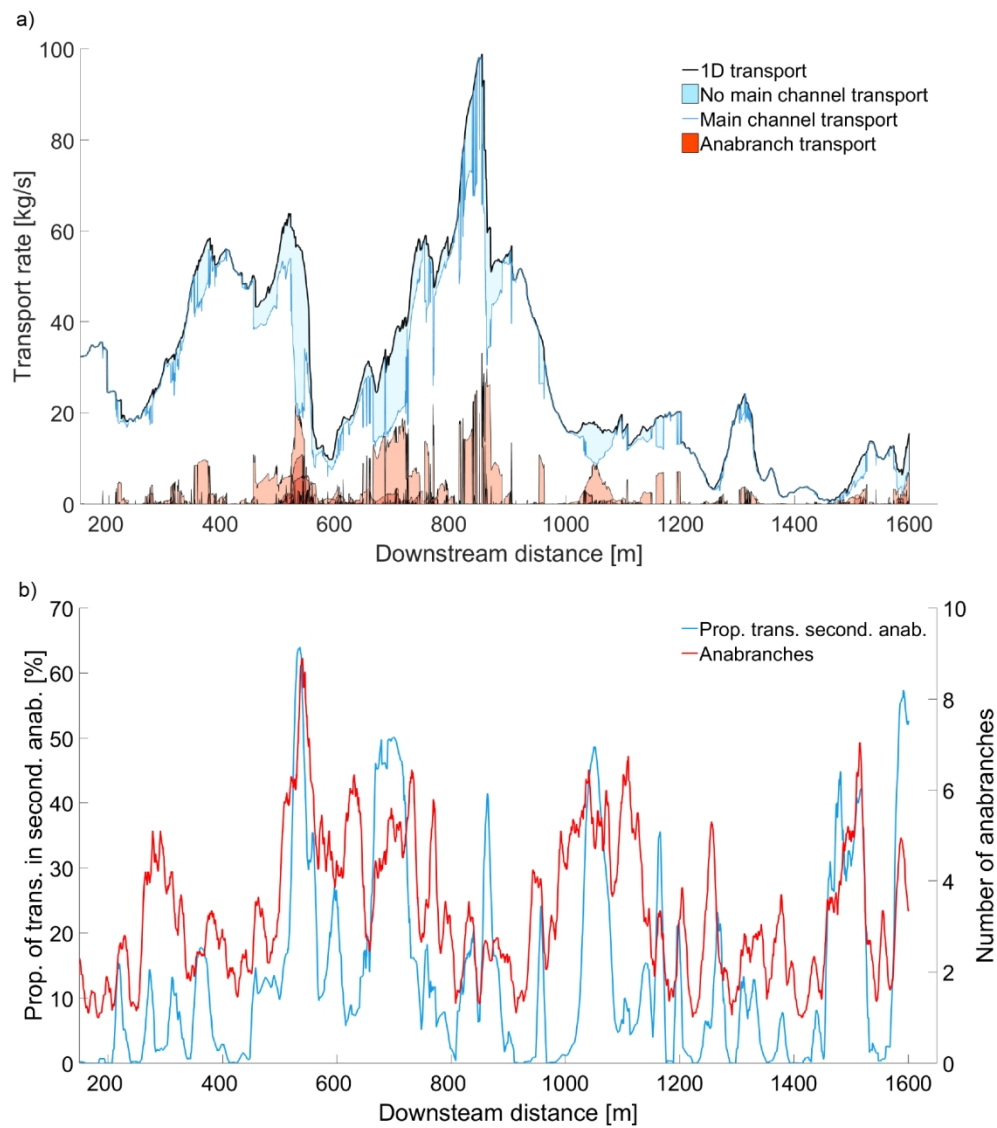51
52
53
54
55
56
57
58
59
60

Figure 11. a) contribution of each anabranch to the total transport rate for period 3rd to 4th of August (period 2 in Table 2); b) Proportion of transport taking place in secondary anabranches [%] is positively correlated with the number of anabranch per cross-section (r = 0.52, p < 0.05). Note that a 20 m moving mean was applied in the figure on the different curves for visualisation purposes.

1
2
3
4
5
6
7
8
9
10
11
12
13
14
15
16
17
18
19
20
21
22
23
24
25
26
27
28
29
30
31
32
33
34
35
36
37
38
39
40
41
42
43
44
45
46
47
48
49
50
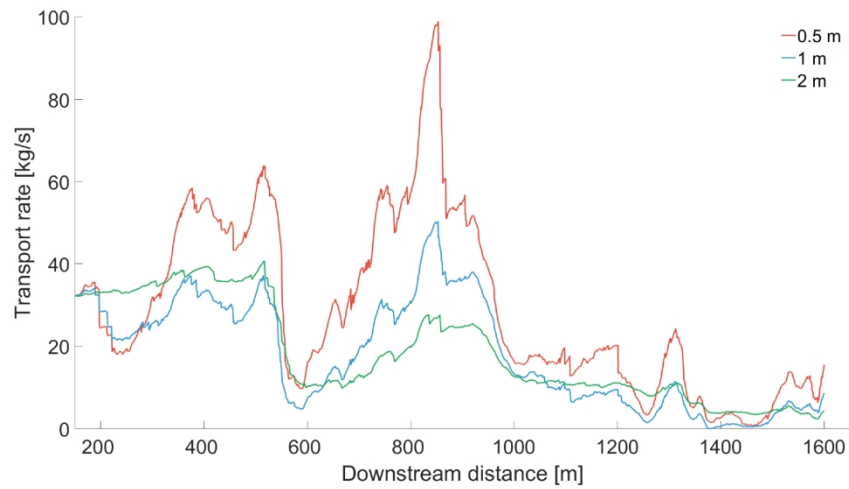51
52
53
54
55
56
57
58
59
60

Figure 12. 1D transport rates calculated for the period 3rd to 4th of August (period 2 in Table 2) with DEM resolutions of 0.5 m, 1 m and 2 m. Note that a 20 m moving mean was applied tin the figure on the different curves for visualisation purposes.

1
2
3
4
5
6
7
8
9
10
11
12
13
14
15
16
17
18
19
20
21
22
23
24
25
26
27
28
29
30
31
32
33
34
35
36
37
38
39
40
41
42
43
44
45
46
47
48
49
50
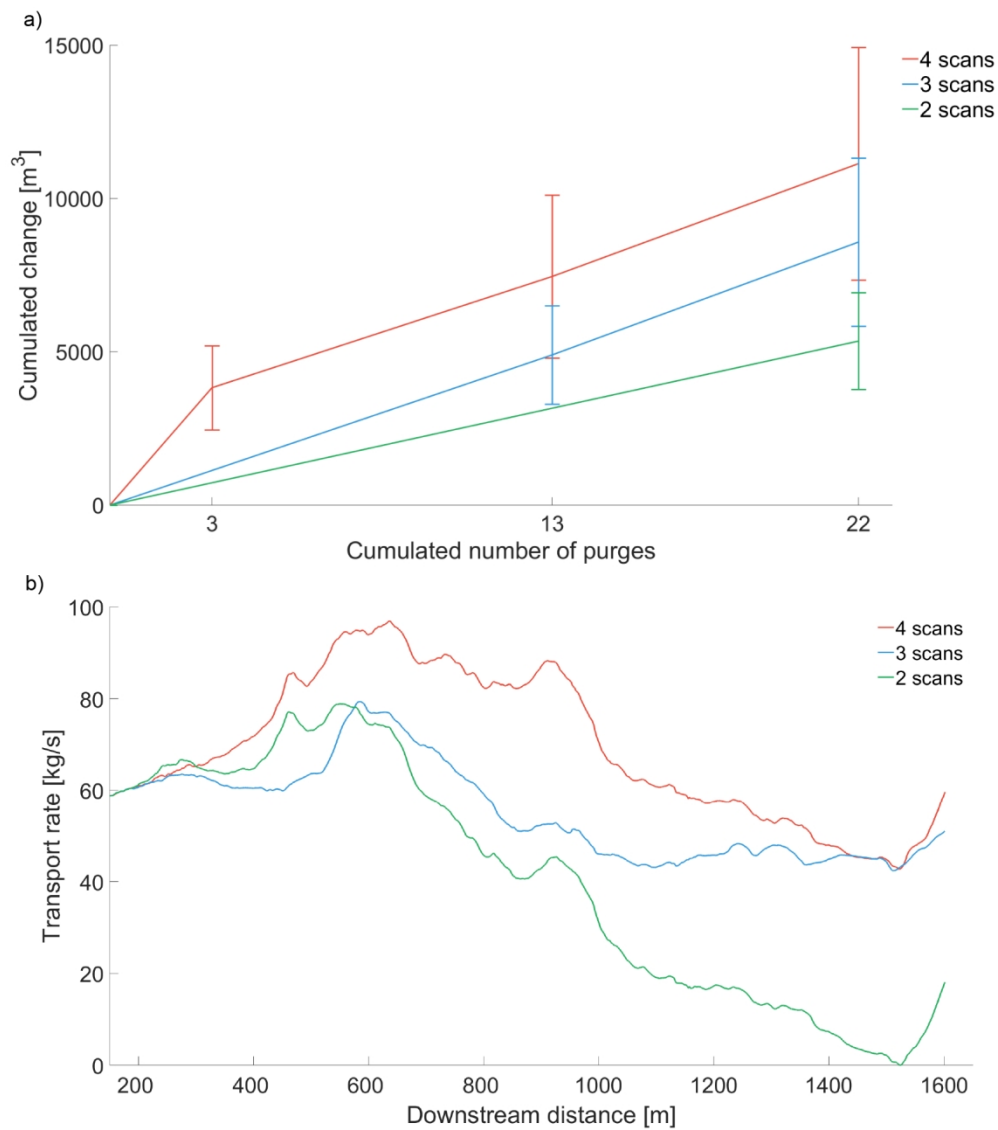51
52
53
54
55
56
57
58
59
60

Figure 13. a) Effect of scan frequency and number of flushing events upon the gross volume change and b) Upon 1D transport rates. Overall, the greater the number of flushing events, the more likely the compensating scour-fill effect and the smaller the derived morphological changes and transport rates. Note that a 20 m moving mean was applied tin the figure on the different curves for visualisation purposes.